nature plants

ARTICLES

https://doi.org/10.1038/s41477-020-00787-9

Genetic elucidation of interconnected antibiotic pathways mediating maize innate immunity

Yezhang Ding[1,15], Philipp R. Weckwerth[1,15], Elly Poretsky[1], Katherine M. Murphy[2], James Sims[3], Evan Saldivar[1], Shawn A. Christensen[4], Si Nian Char[5], Bing Yang[5,6], Anh-dao Tong[1], Zhouxin Shen[1], Karl A. Kremling[7], Edward S. Buckler[7,8], Tom Kono[9], David R. Nelson[10], Jörg Bohlmann[11], Matthew G. Bakker[12,13], Martha M. Vaughan[12], Ahmed S. Khalil[1], Mariam Betsiashvili[1], Keini Dressano[1], Tobias G. Köllner[14], Steven P. Briggs[1], Philipp Zerbe[2], Eric A. Schmelz[1] and Alisa Huffaker[1]✉

Specialized metabolites constitute key layers of immunity that underlie disease resistance in crops; however, challenges in resolving pathways limit our understanding of the functions and applications of these metabolites. In maize (*Zea mays*), the inducible accumulation of acidic terpenoids is increasingly considered to be a defence mechanism that contributes to disease resistance. Here, to understand maize antibiotic biosynthesis, we integrated association mapping, pan-genome multi-omic correlations, enzyme structure–function studies and targeted mutagenesis. We define ten genes in three zealexin (*Zx*) gene clusters that encode four sesquiterpene synthases and six cytochrome P450 proteins that collectively drive the production of diverse antibiotic cocktails. Quadruple mutants in which the ability to produce zealexins (ZXs) is blocked exhibit a broad-spectrum loss of disease resistance. Genetic redundancies ensuring pathway resiliency to single null mutations are combined with enzyme substrate promiscuity, creating a biosynthetic hourglass pathway that uses diverse substrates and in vivo combinatorial chemistry to yield complex antibiotic blends. The elucidated genetic basis of biochemical phenotypes that underlie disease resistance demonstrates a predominant maize defence pathway and informs innovative strategies for transferring chemical immunity between crops.

At present, 50% of global arable land is allocated to agriculture. In the absence of yearly improvements in cereal germplasm and productivity, comparable land consumption today would be greater than 60% (refs. [1,2]). Given human reliance on maize (*Zea mays*) and a few related grasses, genetically encoded mechanisms that provide stress protection have been sought[3–5]. In particular, fungal diseases—such as those caused by *Fusarium* species including *Fusarium graminearum*—are widely devastating to poaceous crops, and further result in grain contamination with harmful mycotoxins[6,7]. Understanding the innate immune responses, genetic variation and endogenous pathway interactions that underlie broad-spectrum disease resistance[8] represents foundational knowledge that is necessary for sustained crop improvement and trait optimization.

Plants are protected from pest and pathogen attack by interconnected layers of physical barriers, pattern-recognition receptors, defence proteins and bioactive specialized metabolites[9–11]. Specialized metabolic pathways are often unique to individual species, display specificity in regulated production and mediate cryptic, albeit impactful, phenotypes[9,12]. Benzoxazinoids (BXs) are the most broadly shared and widely studied poaceous chemical defences. Constitutively produced in seedlings, BXs contribute to resistance against insects and fungi, such as northern corn leaf blight (*Setosphaeria turcica*)[5,13–15]. In contrast to BXs and other largely constitutive defences that are present before attack, many specialized metabolites are produced exclusively on demand, are highly localized to the site of challenge and often evade analytical detection[16]. Maize relies on a combination of dynamically regulated BXs, phenylpropanoids and terpenoids for biotic and abiotic stress protection[5,17–19]. Although the biosynthesis and roles of BXs and terpene volatiles in anti-herbivore defences are increasingly understood[13,20], the genetic and biochemical complexities that underlie maize protection against fungal pathogens have remained a challenge to resolve[18,21–23].

Terpenoids are the most structurally diverse class of plant specialized metabolites, and are typically produced from the combined activities of terpene synthase (TPS) and cytochrome P450 monooxygenase (P450) enzymes[24,25]. Many catalytic activities and biological roles have been assigned to the 43 TPSs encoded in the maize B73 genome[26,27]. Known maize terpenoid antibiotics include

[1]Section of Cell and Developmental Biology, University of California at San Diego, La Jolla, CA, USA. [2]Department of Plant Biology, University of California Davis, Davis, CA, USA. [3]ETH Zurich, Institute of Agricultural Sciences, Zurich, Switzerland. [4]Chemistry Research Unit, Center for Medical, Agricultural and Veterinary Entomology, Department of Agriculture, Agricultural Research Service, Gainesville, FL, USA. [5]Division of Plant Sciences, Bond Life Sciences Center, University of Missouri, Columbia, MO, USA. [6]Donald Danforth Plant Science Center, St Louis, MO, USA. [7]Department of Plant Breeding and Genetics, Cornell University, Ithaca, NY, USA. [8]Robert W. Holley Center for Agriculture and Health, Ithaca, US Department of Agriculture, Agricultural Research Service, New York, NY, USA. [9]Minnesota Supercomputing Institute, University of Minnesota, Minneapolis, MN, USA. [10]University of Tennessee Health Science Center, Memphis, TN, USA. [11]Michael Smith Laboratories, University of British Columbia, Vancouver, British Columbia, Canada. [12]National Center for Agricultural Utilization Research, US Department of Agriculture, Agricultural Research Service, Peoria, IL, USA. [13]Department of Microbiology, University of Manitoba, Winnipeg, Manitoba, Canada. [14]Max Planck Institute for Chemical Ecology, Jena, Germany. [15]These authors contributed equally: Yezhang Ding, Philipp R. Weckwerth. ✉e-mail: ahuffaker@ucsd.edu

sesquiterpenoids, which are represented by zealexins (ZXs) and α/β-costic acids[28,29], and diterpenoids, such as kauralexins and dolabralexins[18,30]. Although enzymes that are active in the oxidation of β-selinene to β-costic acid remain unknown, separate studies have demonstrated that both *Zm*CYP71Z16 and *Zm*CYP71Z18 have the ability to oxidize diverse hydrocarbon olefins to yield ZXs, kauralexins and dolabralexins[18,30,31]. Despite advances in elucidating the diterpenoid biosynthetic pathways[18], acidic sesquiterpenoid derivatives of β-macrocarpene, termed ZXs, represent the single-largest class of defensive terpenoids that are known in the genus *Zea*[29], and yet remain the least understood. Highly localized to the site of elicitation, ZX accumulation correlates with the expression of the β-macrocarpene synthase-encoding transcripts Zm*TPS6* and Zm*TPS11*, which display substantial increases after challenge with diverse fungal pathogens[29,32–34]. Consistent with their roles in crop protection, virus-induced gene silencing of Zm*TPS6*/*11* revealed that they are required for restricting smut fungus (*Ustilago maydis*) infection and tumour formation[35]. Although correlations between Zm*TPS6*/*11* transcripts, ZX production and fungal resistance exist[29,35], no single biosynthetic pathway node has been proven in planta, and all known maize lines produce ZXs. Moreover, the structural diversity of ZXs, range of ZX pathway genes and endogenous protective functions remain unresolved[30,31]. Recent advances in -omic tools, coregulation analyses, genetic resources, in vivo protein biochemistry and gene-editing approaches now enable the critical examination and engineering the complex protective pathways that underlie crop resistance.

To define the genetic basis and pan-genome complexity that underlie maize biochemical immunity, here we identified 17 metabolites that are products of the core *Zx* gene network (*Zx1* to *Zx10*). This network consists of three functionally distinct gene clusters that encode TPSs responsible for hydrocarbon olefin production and P450s in the CYP71Z and CYP81A families that facilitate oxygenation and desaturation. ZXs occur within a larger interconnected metabolic network that also produces kauralexins, dolabralexins and α/β-costic acids. Diverse precursors for each family converge on a single node of catalytically promiscuous CYP71Z enzymes that act on multiple endogenous substrates with partially overlapping functions to generate diverse products that can be subsequently decorated further by pathway-specific enzymes. The result is a broad cocktail of metabolites that are generated by a modest number of enzymes through an hourglass-shaped pathway. Metabolic complexity is only one layer of induced responses—after fungal challenge, ZX production co-occurs with changes in half of the measurable proteome. Despite this complexity, analyses of *zx1 zx2 zx3 zx4* quadruple mutants, which are abolished in ZX biosynthesis, demonstrate substantial protective roles against multiple pathogens. Given that all plants produce terpenoid precursors, the promiscuous enzyme activities described here are amenable to genetic transfer. A foundational understanding of genetic and biochemical mechanisms in maize lays the groundwork for diversifying the chemical defences that underlie disease-resistance phenotypes in phylogenetically distant grain crops[36].

Results

Maize harbours a functionally variable gene cluster of four β-macrocarpene synthases. Two pathogen-regulated β-macrocarpene synthases, termed TPS 6 and TPS 11, were previously assigned as the B73 (RefGen_V4) genes *Zm00001d024207* and *Zm00001d024210* (www.maizegdb.org), respectively[32,33]. Current indirect evidence supports that *Zm*TPS6/11 has a role in the production of diverse antibiotics, termed ZXs[29,34]. As a visual aid, we summarized the biochemicals, genes and proteins with examined relevance to the ZX pathway that are present in the genus *Zea* (Supplementary Figs. 1 and 2 and Supplementary Tables 1–4). Analyses of the B73 genome for all TPSs reveal that Zm*TPS6*/*11* are components of a four-gene cluster[37] on chromosome 10 (Fig. 1a), sharing >84% protein identity with each other (Supplementary Figs. 3 and 4). Following the BX pathway nomenclature[5], we adopted unified B73 ZX pathway abbreviations, starting with *Zx1*/*TPS6* (*Zm00001d024207*), *Zx2*/*TPS12* (*Zm00001d024208*), *Zx3*/*TPS11* (*Zm00001d024210*) and *Zx4*/*TPS13* (*Zm00001d024211*) on the basis of sequential chromosome order (Fig. 1a,b). Unless otherwise noted, gene and protein abbreviations refer to B73 (RefGen_V4) reference sequences. RNA sequencing (RNA-seq) analyses of stems from B73, Mo17 and W22 inbred lines, damaged either alone or additionally treated with heat-killed *Fusarium*, demonstrate that fungal-elicited transcript accumulation occurs in an inbred-specific manner (Fig. 1c–e and Supplementary Table 2). To understand the contribution of *Zx* gene cluster I to the production of β-bisabolene and β-macrocarpene, individual genes *Zx1* to *Zx4* from both B73 and W22 lines (Supplementary Figs. 4 and 5 and Supplementary Table 4) were functionally analysed using transient, *Agrobacterium*-mediated expression in *Nicotiana benthamiana*. Expression of B73 (ZX1, ZX3, ZX4) and W22 (ZX2, ZX3, ZX4) revealed similar, albeit different, combinations of functional β-macrocarpene synthases, yielding low levels of β-bisabolene (Fig. 1f,g). In both cases, the lack of β-bisabolene and β-macrocarpene production by W22 ZX1 and B73 ZX2 occurred during otherwise sufficient transcript expression (Supplementary Fig. 5).

To understand common mutations that cause a loss of function in ZX1 to ZX4, we examined amino acid sequence variations in W22 ZX1 and we observed a W274R substitution that is predicted to negatively impact the catalytic site[38] (Supplementary Fig. 4). Reversion of inactive W22 ZX1 back to R274W or mutation of active W22 ZX4 (R274) to W274R reactivated and inactivated, respectively, the enzymes in *N. benthamiana* transient expression assays (Supplementary Fig. 6). W22-like *Zx1* non-synonymous single-nucleotide polymorphisms (SNPs) at chromosome 10 position 56448050 (A to G) that underlie the ZX1 W274R null mutation are common in maize germplasm and are present in >10% of examined inbreds[39,40] (Supplementary Table 5). Analysis of *Zx* gene cluster I in 28 maize genomes demonstrates that predicted β-macrocarpene synthase genes typically exist as four copies but can vary from three to six copies in select inbred lines (Supplementary Figs. 7 and 8, and Supplementary Tables 6 and 7). Beyond functional variation in *Zx1*, we observed that B73 and eight additional inbred lines (32%) contain *Zx2* mutations that are predicted to result in non-functional enzymes (Supplementary Tables 6 and 7). In our analyses here, the lack of significant Mo17 *Zx2* transcript after elicitation (Fig. 1e) corresponds to the absence of detectable Mo17 *Zx2* nucleotides on the basis of gene cluster analyses (Supplementary Fig. 7).

To demonstrate endogenous relationships, we used mutual-rank-(MR)-based global gene coexpression analyses to associate transcriptional patterns of maize sesquiterpene synthases in a large RNA-seq dataset[40]. Analyses revealed that the highest degree of coregulation between *Zx1* and *Zx3*, and between *Zx2* and *Zx4* together with partial Zm*TPS21* coregulation is responsible for β-selinene derived antibiotics[28] (Fig. 1h). Genome-wide analyses of *Zx1* to *Zx4* expression levels in diverse inbred lines are consistent with the complex patterns (Fig. 1i) witnessed in B73, Mo17 and W22 (Fig. 1c–e). Analyses of *Zx* gene cluster I demonstrate that inbred-line-specific combinations of functional ZX1 to ZX4 proteins are common (Supplementary Fig. 7) and contribute to β-bisabolene and β-macrocarpene production (Fig. 1a–i).

A second *Zx* gene cluster contains and encodes three promiscuous CYP71Z-family cytochrome P450s. Increases in *Zx1* to *Zx4* accumulation are among the largest fold changes in transcription after pathogen challenge[29,32]. In an early analysis of stems, we observed that a member of the cytochrome P450 CYP71 family, Zm*CYP71Z18* (NM_001147894), is among the most *F. graminearum*

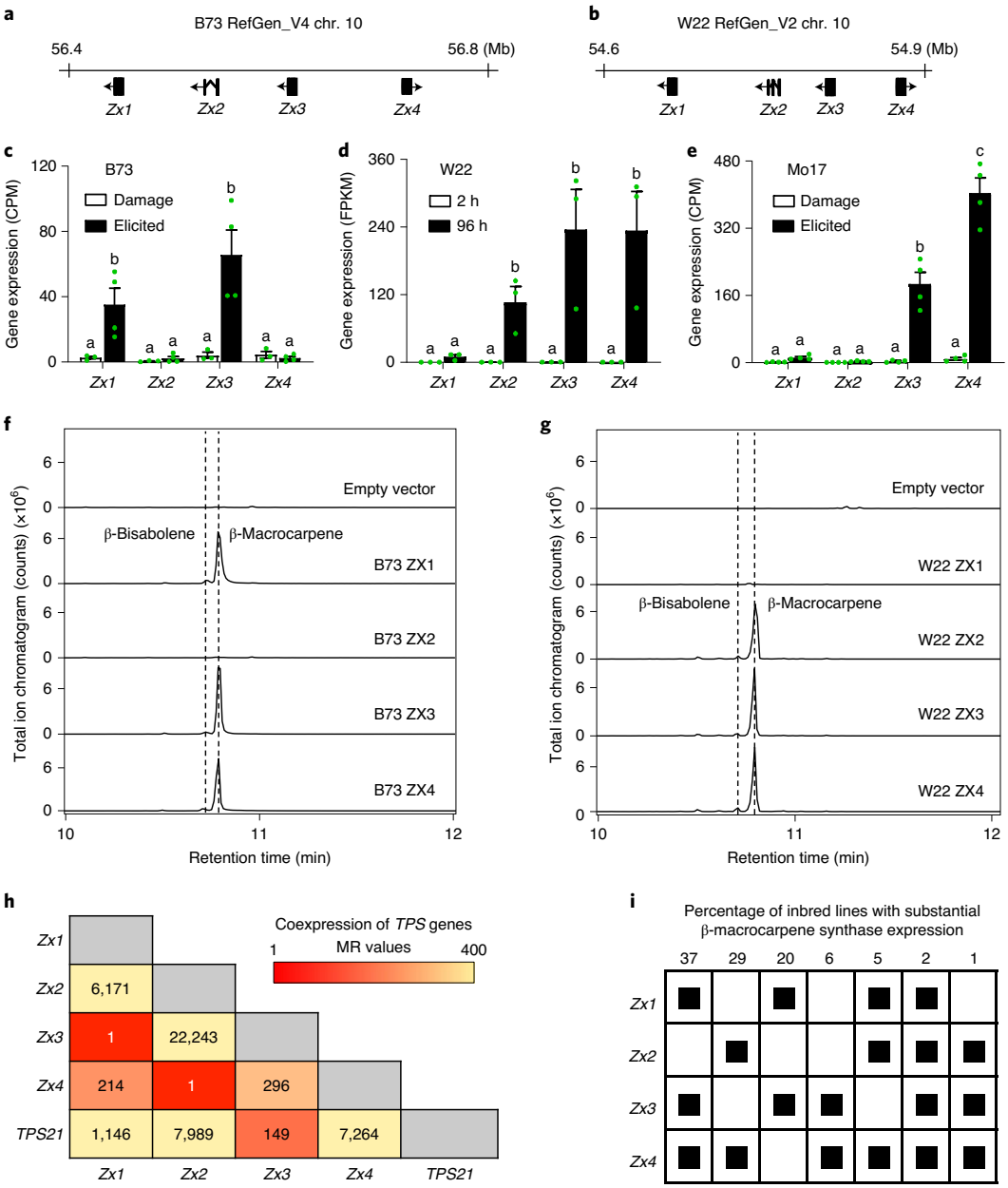

Fig. 1 | A genetically variable cluster of four maize TPSs ensures the production of ZX precursors. a–e, Tandem array of four β-macrocarpene synthase genes, termed *Zx1* to *Zx4*, on chromosome (chr.) 10 of the B73 genome (RefGen_V4) (**a**) and the W22 genome (RefGen_V2) (**b**). *Zx1* to *Zx4* transcript abundance derived from RNA-seq analyses of five-week-old B73 (**c**), W22 (**d**) and Mo17 (**e**) stems damaged (damage) only or additionally treated with heat-killed *F. venenatum* hyphae (elicited). For Mo17 and B73, harvests were performed at 36 h and 3′ RNA-seq gene expression is given as counts per million mapped reads (CPM). For W22 RNA-seq results, the average of three early (0 h, 2 h and 4 h) and late (72 h, 96 h and 120 h) elicitation time points with gene expression is given as fragments per kilobase of transcript per million mapped reads (FPKM). For **c**–**e**, data are mean ± s.e.m. B73 damaged, $n = 3$ biologically independent samples; B73 elicited, $n = 4$ biologically independent samples; Mo17 damaged and elicited, $n = 4$ biologically independent samples. Within plots, different letters (a–c) represent significant differences; statistical analysis was performed using one-way analysis of variance (ANOVA), $P < 0.05$; Tukey tests were used to correct for multiple comparisons, $P < 0.05$. **f**,**g**, GC–MS total ion chromatograms are shown for leaf volatiles emitted after *Agrobacterium*-mediated transient *N. benthamiana* expression assays of B73 (**f**) and W22 (**g**) encoded β-macrocarpene synthases ZX1, ZX2, ZX3 and ZX4. An empty vector was used for the *Agrobacterium*-infiltrated control. Four biological repeats were performed and showed similar results. **h**, Heat map of the coexpression of *Zx1, Zx2, Zx3, Zx4* and an β-selinene synthase (Zm*TPS21*) present in a dataset of 1,960 RNA-seq samples. The low numbers in the squares (<250) indicate supportive MR scores. **i**, Expression matrix of *Zx1* to *Zx4* in 100 inbred lines from a dataset of 1,960 RNA-seq samples. Individual *Zx1, Zx2, Zx3* and *Zx4* transcripts with expression levels of ≥5% of the total sum expression of *Zx1* to *Zx4* were counted as expressed and are represented by filled black squares. The empty white squares indicate low levels of gene expression (<5% of the sum of *Zx1* to *Zx4* expression).

upregulated genes that co-occurred with *Zx1* to *Zx4* members[29]. Subsequently, both *Zm*CYP71Z18 and the adjoining *Zm* CYP71Z16 were shown to be catalytically active in the oxidation of β-macrocarpene to ZA1 (refs. [30,31]). To consider roles for additional P450s, we performed a global gene coexpression analysis of the summed expression of *Zx1* to *Zx4* with all of the predicted maize

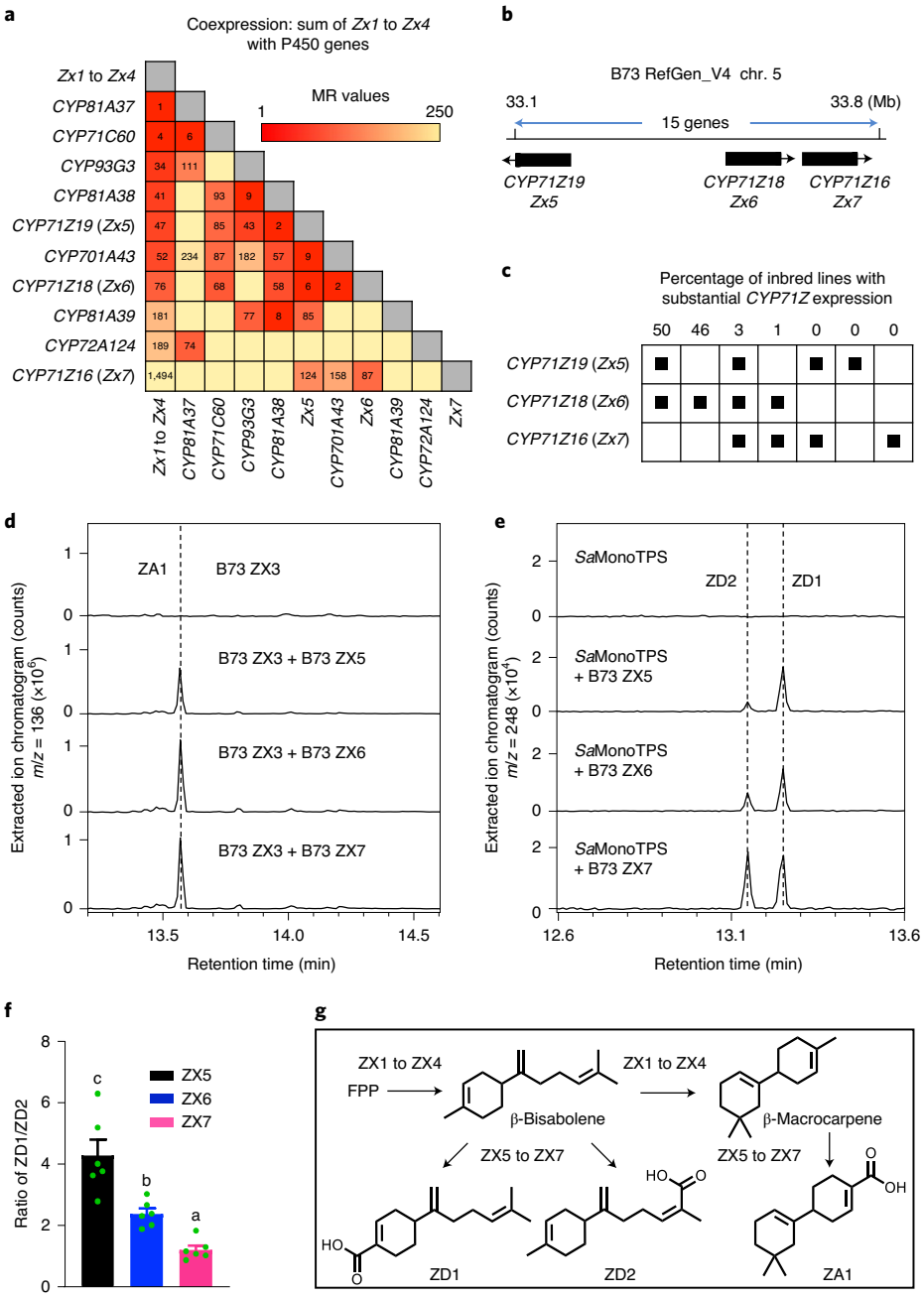

Fig. 2 | *Zx* gene cluster II contains three 71Z-family cytochrome (CYP) P450s that catalyse the production of A- and D-series ZXs. a, Heat map of the summed expression of *Zx1* to *Zx4* and coexpression with all maize P450s in a dataset of 1,960 RNA-seq samples. The low numbers in the squares (<250) indicate supportive MR scores. Weak MR correlations of >250 were omitted. **b**, The physical position of the chromosome 5 gene cluster containing Zm*CYP71Z19* (*Zx5*), Zm*CYP71Z18* (*Zx6*) and Zm*CYP71Z16* (*Zx7*) referenced to the B73 genome (RefGen_V4). **c**, Expression matrix of *Zx5*, *Zx6* and *Zx7* in 100 inbred lines present in a dataset of 1,960 RNA-seq samples. Genes with expression levels of ≥5% of the sum *Zx5* to *Zx7* expression were counted as being expressed (filled black squares). **d**, GC–MS-extracted ion chromatograms of hexane extracts derived from *Agrobacterium*-mediated transient *N. benthamiana* coexpression assays of ZX3 individually paired with ZX5, ZX6 or ZX7 all resulted in the production of ZA1. **e**, Parallel coexpression assays and extracted ion chromatograms of the β-bisabolene synthase from *Santalum album* (*Sa*MonoTPS) with ZX5, ZX6 or ZX7 all resulted in the production of ZD1 and ZD2 in variable proportions. Four biological repeats were performed and showed similar results. **f**, Ratios of ZD1 to ZD2 from *Agrobacterium*-mediated transient *N. benthamiana* coexpression assays of *Sa*MonoTPS with ZX5, ZX6 or ZX7. Data are mean ± s.e.m. $n = 6$ biologically independent replicates. Different letters (a–c) represent significant differences; statistical analysis was performed using one-way ANOVA, $P < 0.05$; Tukey tests were used to correct for multiple comparisons, $P < 0.05$. **g**, Schematic of farnesyl pyrophosphate (FPP) cyclization reactions catalysed by ZX3 (a β-bisabolene-dependent β-macrocarpene synthase) and ZX5, ZX6 and ZX7 each yield ZD1, ZD2 and ZA1.

P450 transcripts and found nine candidates with low MR scores (<250), including Zm*CYP71Z18* and Zm*CYP71Z19* (Fig. 2a), that were further supported by replicated RNA-seq data (Supplementary Table 2). Zm*CYP71Z19* is phylogenetically most closely related to Zm*CYP71Z16/18* (ref. [18]) and is located within the same 15-gene interval on chromosome 5 (Fig. 2b and Supplementary Fig. 9).

Similar to *Zx1* to *Zx4*, Zm*CYP71Z16*/*18*/*19* each display variable relative expression between inbred lines (Fig. 2c). We name the B73 P450 genes Zm*CYP71Z19* (*Zm00001d014121*) *Zx5*, Zm*CYP71Z18* (*Zm00001d014134*) *Zx6* and Zm*CYP71Z16* (*Zm00001d014136*) *Zx7* on the basis of chromosome order, with each sharing >71% protein sequence identity (Supplementary Fig. 10). Gene-cluster-II analyses of 28 maize genomes identified only modest variation but, interestingly, a single inbred line (CML228) contains duplications of *Zx5*, *Zx6* and *Zx7* to yield a total of six *CYP71Z*-family genes (Supplementary Figs. 8 and 11, and Supplementary Tables 6 and 7). Consistent with a shared role in ZX biosynthesis, *Agrobacterium*-mediated enzyme coexpression assays with B73 ZX3 in *N. benthamiana* demonstrate that ZX5, ZX6 and ZX7 each independently catalyse the oxidization of β-macrocarpene to ZA1 (Fig. 2d,g), supporting pathway redundancy.

As a less abundant product of ZX1 to ZX4 (Fig. 1f,g and Supplementary Fig. 5), β-bisabolene predictably contributes to the array of 13 established candidate ZXs[29,33]. Importantly, levels of β-bisabolene production by β-macrocarpene synthases vary, and alterations in pH and Mn^{2+} availability can result in the coequal production β-bisabolene and β-macrocarpene by ZX1 (*Zm*TPS6) when expressed in *E. coli*[33]. Diseased maize sheath tissue was used to purify, isolate and NMR-identify two acidic β-bisabolene derivatives, namely zealexin D1 (ZD1; 4-(6-methylhepta-1,5-dien-2-yl) cyclohex-1-ene-1-carboxylic acid) and ZD2 (2-methyl-6-(4-methylcyclohex-3-en-1-yl)hepta-2,6-dienoic acid), that produce diagnostic gas chromatography coupled mass spectrometry (GC–MS) electron ionization (EI) spectra as methyl ester derivatives (Supplementary Table 8 and Supplementary Fig. 12). To specifically examine the catalytic oxidation of β-bisabolene, we performed *N. benthamiana* coexpression assays using *Santalum album* mono TPS (*Sa*MonoTPS, EU798692), which utilizes the precursor *E*/*E*-farnesyl diphosphate (FDP) to produce β-bisabolene[41]. Similar to ZA1 biosynthesis, ZX5, ZX6 and ZX7 each catalysed the complete oxidation of β-bisabolene at the C1 and C15 positions, yet resulted in significant differences in the final ratios of ZD1/ZD2 produced (Fig. 2d–f and Supplementary Fig. 13). Our collective findings demonstrate that ZX6 and ZX7 support promiscuous catalytic activity on established ZX1 to ZX4 products (Fig. 1f,g) and also diterpenoid defence precursors *ent*-isokaurene (Supplementary Fig. 14) and dolabradiene[18,30]. ZX5 enzyme coexpression analyses demonstrate activity on sesquiterpene olefins, (Fig. 2d,e) further including conversion of the substrate β-selinene to β-costic acid (Supplementary Fig. 14); however, no appreciable activity in kauralexin biosynthesis was found[18,28] (Supplementary Fig. 14). As previously observed maize sesquiterpene acids, termed analytes 2 and 4 (ref. [29]), our results clarify that low levels of β-bisabolene-derived ZD2 and ZD1 co-occur with A, B and C-series ZXs.

To consider the evolutionary origin and catalytic potential of *Zx* gene cluster II, we examined the single-copy *Sorghum bicolor* gene (*Sobic.001G235500*) Sb*CYP71Z19*, which exists as a ZX5 syntenic orthologue sharing 89% amino acid identity (Supplementary Fig. 9) despite at least 12 million years[42] of phylogenetic divergence between the two genera. Both maize and *Sorghum* gene evolution estimates (Supplementary Fig. 15) and enzyme coexpression studies—which demonstrate that *Sb*CYP71Z19 can oxidize both sesquiterpene and diterpene precursors (Supplementary Fig. 14)—are consistent with the existence of a *CYP71Z* progenitor gene that possessed sufficient promiscuity to produce diverse terpenoid defences before gene duplication and divergence in maize. Similarly, highland teosinte (*Z. mays* spp. *mexicana*) contains only two *CYP71Z* genes near cluster II, and they are most similar to *Zx5* and *Zx7* (Supplementary Fig. 11).

To consider whether gene cluster II provides endogenous ZX pathway redundancy, we examined the W22 *zx5 Ds* insertion mutant (*dsgR102G05*) for fungal-elicited ZXs and found no measurable deficits (Supplementary Fig. 16). While suggestive, the absence of an altered ZX chemotype requires a detailed characterization of W22 *zx5* (*dsgR102G05*) at the transcriptional and enzymatic level before any potential impact of the transposon insertion can be stated with certainty. Of *Zx5* to *Zx7*, *Zx5* displays the highest degree of genome-wide coregulation with *Zx1* to *Zx4* (Fig. 2a) as well as the greatest degree of catalytic specificity towards sesquiterpene substrates (Supplementary Fig. 14). Our results support that enzyme promiscuity and gene-cluster-II redundancy enable partially interchangeable enzymes to be shared by at least four different maize defence pathways[18,30].

Forward genetics reveals a third *Zx* biosynthetic gene cluster. Beyond carboxylic acid derivatives, ZXs contain additional oxidations, desaturations and aromatized variants[29]. To identify the enzyme(s) that are responsible for these modifications, we screened germplasm for differences in fungal-elicited ratios of ZB1 to ZA1 and focused on inbred lines that have previously been used for biparental crosses in the establishment of mapping populations[43,44]. Compared with other examined inbred lines, Mo17 uniquely displays low ZB1/ZA1 ratios (Fig. 3a). Using the intermated B73 × Mo17 (IBM) recombinant inbred lines (RILs)[43], we used the ratio of ZB1/ZA1 as a mapping trait in mature field roots and identified highly significant SNPs on chromosome 1 (Fig. 3b and Supplementary Table 9). Similarly, a genome-wide association study using the Goodman association panel[39] further supported colocalized SNPs (Supplementary Fig. 17) spanning the same interval.

To systematically narrow candidates, near-isogenic lines (NILs) derived from B73 and Mo17 (ref. [45]) were used for fine-mapping, and resulted in a narrow 100 kb region containing three B73 *CYP81A* genes (Fig. 3c–e) named Zm*CYP81A37* (*Zm00001d034095*) *Zx8*, Zm*CYP81A38* (*Zm00001d034096*) *Zx9* and Zm*CYP81A39* (*Zm00001d034097*) *Zx10*. MR analyses of the combined expression of *Zx1* to *Zx4* and *Zx5* to *Zx7* in relation to the mapping interval confirmed strong *Zx*-pathway coexpression (Fig. 3d). In contrast to B73, the Mo17 genome uniquely contains an 8 kb insertion in *Zx8* (Fig. 3f) and the Mo17 *Zx8* transcript displays no fungal-elicited accumulation (Fig. 3g). In the B73 genome, ZX8 shares 99% and 72% amino acid identity with ZX9 and ZX10, respectively (Supplementary Fig. 18).

To examine gene functions, combinations of the representative B73 pathway genes *Zx3* and *Zx6* were coexpressed in *N. benthamiana* with combinations of *Zx8*, *Zx9* and *Zx10*. Both ZX8/9 pairings resulted in the hydroxylation of ZA1 at carbon C1 to produce ZA2, hydroxylation at C6 to produce ZA5 (2-hydroxy-5′,5′-dimethyl-[1,1′-bi(cyclohexane)]-1′,3-diene-4-carboxylic acid), desaturation of the C1–C6 bond resulting in ZB1 and the predicted autoaromatization product ZC1 (Fig. 4a,b, Supplementary Figs. 12 and 13, and Supplementary Table 8). ZX10 resulted in the hydroxylation of ZA1 at the C8 position to yield ZA3. Parallel microbial coexpression of B73 enzymes ZX3 and ZX7 with ZX8 and ZX9 in *E. coli* also demonstrated the conversion of ZA1 to ZB1, while ZX10 similarly produced ZA3 (Supplementary Fig. 19). In *N. benthamiana*, the combined activities of B73 ZX3, ZX6, ZX8/9 and ZX10 yielded the additional additive product termed ZB3 (6′-hydroxy-5′,5′-dimethyl-[1,1′-bi(cyclohexane)]-1,1′,3-triene-4-carboxylic acid; Fig. 4a,b, Supplementary Figs. 12 and 13 and Supplementary Table 8) and low levels of the aromatic variant ZC2 (refs. [29,46]). Novel and established ZXs produced characteristic retention times and EI spectra when produced in maize and *N. benthamiana* tissues (Supplementary Figs. 12 and 13). Identifications in maize followed from purification and NMR elucidation (Supplementary Table 8). ZX biosynthetic deficiencies in Mo17 are partially explained by a loss of transcript accumulation of *Zx8* but not *Zx9* (Fig. 3g). *N. benthamiana* coexpression of B73 *Zx3* and *Zx6* with Mo17 *Zx9* resulted in equal transcript levels on the basis of quantitative PCR with

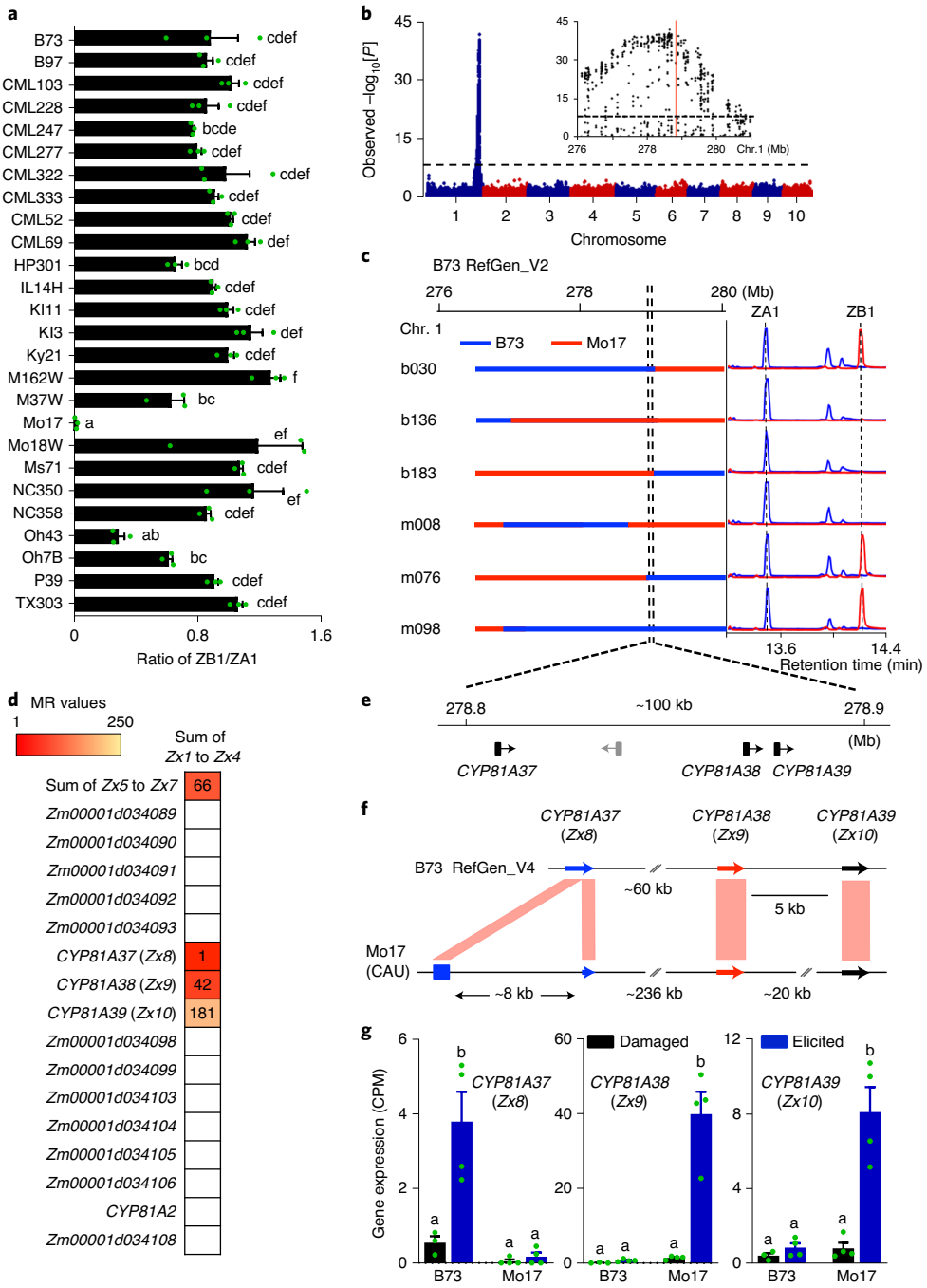

Fig. 3 | Association mapping reveals that *Zx* gene cluster III contains three CYP81A-family P450s. a, The ratio of ZB1 to ZA1 in stems of 25 different four-week-old inbred lines treated with heat-killed *F. venenatum* hyphae for 3 d identified that Mo17 is a unique parent. Data are mean ± s.e.m. $n = 3$ biologically independent samples. **b**, Association analysis of the ratio of ZB1 to ZA1 using the IBM RILs with the general linear model and 173,984 SNPs. The most statistically significant SNPs are located on chromosome 1 (B73 RefGen_V2). The black dashed line denotes the false discovery rate (< 0.05 at $-\log_{10}[P]$) using a Bonferroni correction. Inset: local Manhattan plot surrounding the peak on chromosome 1. The red line denotes the initial estimated position of the candidate gene(s). **c**, B73 and Mo17 chromosomal segments in B73 × Mo17-derived NILs represented by blue and red, respectively, paired with chemotypes indicated as GC–MS-extracted ion chromatograms (ZA1, $m/z = 136$, blue; ZB1, $m/z = 246$, red). **d**, Heat map of the coexpression of genes in the mapping region with the summed expression of *Zx1* to *Zx4* and *Zx5* to *Zx7* present in a dataset of 1,960 RNA-seq samples. The low numbers in the squares (<250) indicate supportive MR scores. Weak MR correlations of >250 were omitted. **e**, The locus was fine-mapped to a 100-kb region on B73 bacterial artificial chromosomes AC202436 and AC196018 on chromosome 1 containing four genes (B73 RefGen_v2). **f**, Tandem array of *CYP81A37* (*Zx8*), *CYP81A38* (*Zx9*), *CYP81A39* (*Zx10*) on chromosome 1 of the B73 genome (RefGen_V4) and the Mo17 genome (China Agricultural University (CAU)). Compared with B73 *Zx8*, Mo17 *Zx8* contains an 8-kb insertion. **g**, 3′ RNA-seq results derived from five-week-old B73 and Mo17 stems that were either damaged or additionally treated with heat-killed *F. venenatum* hyphae (elicited) and harvested 36 h later. Gene expression is given as counts per million mapped reads. Data are mean ± s.e.m. B73 damaged, $n = 3$ biologically independent samples; B73 elicited, $n = 4$ biologically independent samples; Mo17 damaged and elicited, $n = 4$ biologically independent samples. Within the plots, different letters (a–f) represent significant differences; statistical analysis was performed using one-way ANOVA; $P < 0.05$; Tukey tests were used to correct for multiple comparisons; $P < 0.05$.

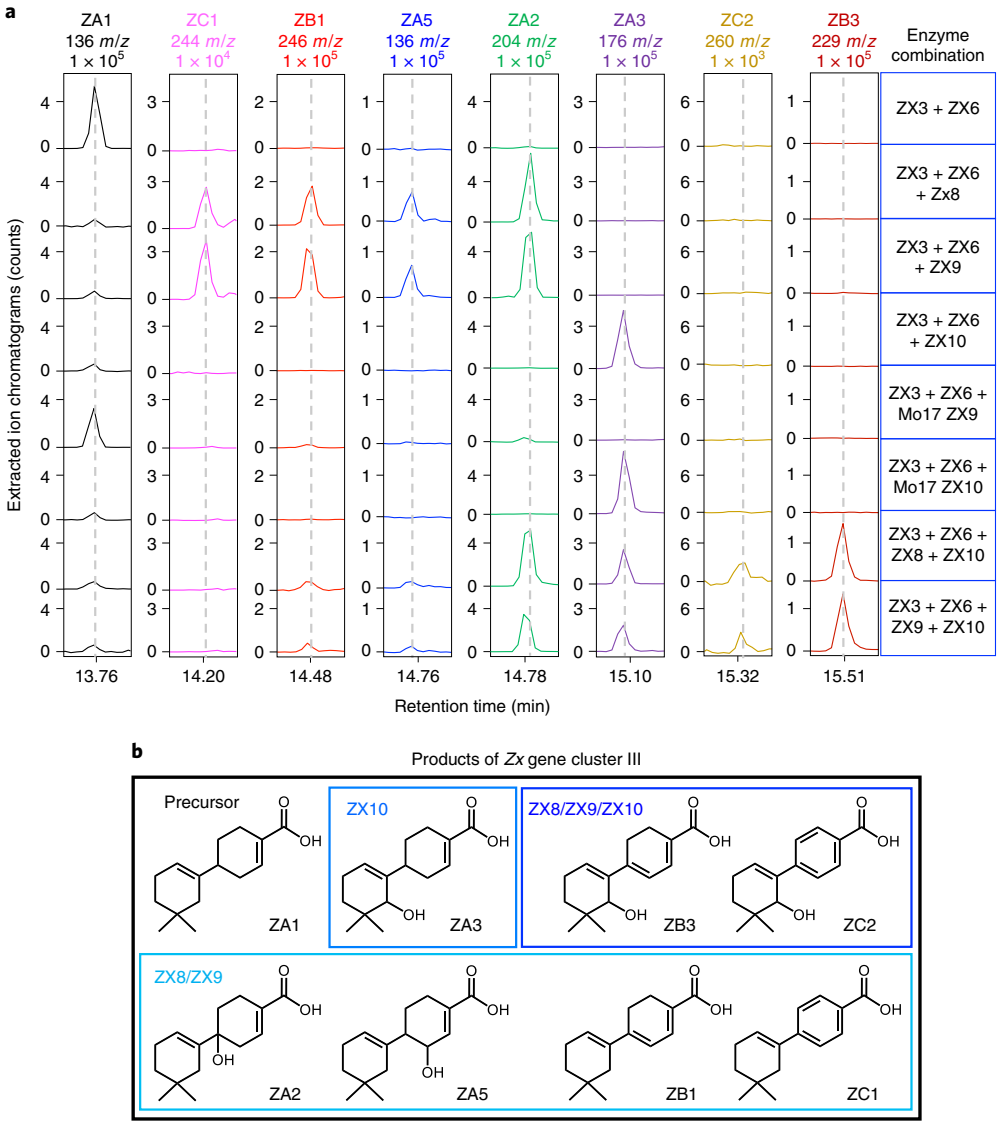

Fig. 4 | Enzyme coexpression defines the role of *Zx* gene cluster III in antibiotic biosynthesis. a, GC–MS-extracted ion chromatograms of extracts derived from *Agrobacterium*-mediated transient *N. benthamiana* enzyme coexpression assays using representative *Zx* pathway genes from gene cluster I (*Zx3*), gene cluster II (*Zx6*) and combinations from gene cluster III, including *Zx8*, *Zx9* and *Zx10*. Combinatorial in vivo enzyme assays in the presence of ZA1 (m/z=136, product of ZX3 and ZX6) yielded seven additional ZXs with diagnostic EI m/z ions as follows: ZC1, m/z=244; ZB1, m/z=246; ZA5, m/z=136; ZA2, m/z=204; ZA3, m/z=176; ZC2, m/z=260; and ZB3, m/z=229. ZA5 and ZB3 represent new compounds. To address the association mapping results, functionality of Mo17 ZX9 was included and supported impaired activity in ZB1 synthesis. In contrast to Mo17 ZX9, Mo17 ZX10 remains fully functional. Four independent experiments were performed and showed similar results. **b**, Structures of ZXs derived from the activity of ZX8, ZX9 and ZX10 on ZA1 as a substrate.

reverse transcription (RT–qPCR) analysis, yet a significant, more than tenfold decrease in ZA2, ZA5 and ZB1 production (Fig. 4a and Supplementary Fig. 20), consistent with separate deleterious mutations in both Mo17 *Zx8* and Mo17 *Zx9*.

To consider roles for ZX8 and ZX9, we purified ZB1 and observed significant antifungal activity against three important maize pathogens, namely *Fusarium verticillioides*, *F. graminearum* and *Aspergillus flavus*, similar to ZA1 (Supplementary Fig. 21). Gene-cluster-III analyses of 28 maize genomes identified select inbred lines that displayed either a contraction or expansion of *Zx8* gene copies yielded a range of 2–5 predicted *Zx* cluster-III genes (Supplementary Figs. 8 and 22, and Supplementary Tables 6 and 7). *Zx* gene cluster III expands the established roles of CYP81 enzymes beyond glucosinolate, isoflavonoid, lignin and xanthone biosynthesis to include sesquiterpenoid antibiotics (Supplementary Fig. 23).

Elicited antibiotic production occurs during large-scale transcriptomic, proteomic and metabolomic reprogramming. For more than 60 years, BXs have been extensively examined as the predominant chemical defences that protect maize seedlings from herbivores and pathogens[5,15,47,48]. To understand the context in which acidic terpenoids predominate, we applied heat-killed *Fusarium venenatum* hyphae to wounded maize stem tissues at 11 d, 25 d and 35 d after planting. After 3 d of elicitation, seedlings (aged 14 d) maintained predominantly BX metabolites, whereas plants aged 38 d displayed predominantly complex mixtures of acidic terpenoids and flavonoids (Fig. 5a). Experimental variables, such as the plant age and stress conditions considered, probably contributed to a historical focus on BX metabolites. To better understand defence activation in mature plants, we conducted a time-course experiment over a period of 120 h after applying heat-killed *Fusarium* hyphae to stem tissues of the

W22 inbred line and measured changes in transcripts, proteins and defence metabolites (Supplementary Tables 1, 2, 10 and 11). Early (0–4 h) versus late (72–120 h) fold changes in protein levels were averaged to provide statistical patterns. A combination of wounding and fungal elicitation resulted in 52% of proteins (5,501 out of 10,508) that displayed either significantly positive (2,694) or negative (2,807) changes in abundance after treatment (Supplementary Table 11). Protein–transcript pairs (10,508) were analysed using complete-linkage hierarchical clustering (Fig. 5b) and assigned to 11 modules (0–10) using weighted gene coexpression network analysis (WGCNA) of protein and RNA fold changes after rank-order normalization (Fig. 5c, Supplementary Fig. 24 and Supplementary Table 11). Many acidic terpenoid and flavonoid biosynthetic pathway genes grouped in module 3 (1,534) containing an enrichment in Gene Ontology (GO) terms relating to response to stimulus and secondary and phenylpropanoid metabolic processes (Fig. 5b,d and Supplementary Tables 11 and 12). Flavonoids are predominantly protective biochemicals in nearly all plants, are fungal-regulated in maize and commonly cooccur with terpenoids[49–51]. The upregulated production of simple flavonoids, such as naringenin and apigenin, is associated with increased protein levels of phenylalanine ammonia lyase, cinnamate 4-hydroxylase, 4-coumarate CoA ligase, chalcone synthase, chalcone isomerase and flavone synthase family members[52], many of which parallel ZX pathway activation (Fig. 5d). In contrast to terpenoid and flavonoid pathways, early BX pathway transcripts and enzymes were assigned to module 1 (4,787) and display rapid cosuppression (Fig. 5c,d and Supplementary Tables 2 and 11). By contrast, the accumulation of more terminal BX metabolites and biosynthetic proteins is pathogen-elicited (Fig. 5d), exists in modules with parallel RNA/protein increases (Supplementary Table 11 and Supplementary Fig. 24) and highlights a shift from general defences to those with increased reactivity[14].

Diverse maize antibiotics produced through an hourglass-shaped biosynthetic pathway drive pathogen resistance. To better understand ZX diversity, we conducted large-scale stem inoculations with a necrotrophic fungal pathogen, namely southern leaf blight (SLB, *Cochliobolus heterostrophus*), and isolated additional related metabolites. Beyond the previously known ZXs[29,34], ZD1, ZD2, ZA5 and ZB3 (Figs. 2 and 4 and Supplementary Table 8), we describe four additional structures, namely ZA6 (1,4′-dihydroxy-5′,5′-dimethyl-[1,1′-bi(cyclohexane)]-1′,3-diene-4-carboxylic acid), ZA7 (4′,6′-dihydroxy-5′,5′-dimethyl-[1,1′-bi(cyclohexane)]-1′,3-diene-4-carboxylic acid), ZA8 (1-hydroxy-5′,5′-dimethyl-4′-oxo-[1,1′-bi(cyclohexane)]-1′,3-diene-4-carboxylic acid) and ZA9 (6′-hydroxy-5′,5′-dimethyl-4′-oxo-[1,1′-bi(cyclohexane)]-1′,3-diene-4-carboxylic acid) (Fig. 6a, Supplementary Table 8, and Supplementary Figs. 12 and 25) derived from β-macrocarpene. In SLB elicitation experiments of maize stem tissues, at least 15 ZX pathway products were detectable, produced diagnostic EI spectra and significantly accumulated over time (Supplementary Figs. 12, 25 and 26).

Our current and collective research[18,28–30,34] enabled the construction of the maize ZX pathway and shared functions (Fig. 6a). Gene duplications resulting in gene clusters I, II and III combine with enzyme promiscuity (Figs. 1, 2 and 4, and Supplementary Fig. 14) to create a complex hourglass pathway in which diverse endogenous substrates of independent origins share enzymes at an intermediate biosynthetic step and subsequently reconnect with pathway-specific enzymes. To examine interactive roles of the *Zx* gene cluster II, we performed a global gene coexpression analysis of the summed expression of *Zx5* to *Zx7* with all predicted maize P450 and TPS transcripts (Supplementary Fig. 27). The results support the strong coexpression of *Zx5* to *Zx7* with ZX (*Zx1*, *Zx2*, *Zx3*, *Zx4* and *Zx9*) and diterpenoid defence pathways (Zm*An2*, Zm*KSL2*, Zm*KO2* and Zm*KSL4*)[18,30] with a limited number of additional TPS and P450s transcripts (Supplementary Fig. 27). Heterologous expression studies in *N. benthamiana* support specificity in late pathway steps. For example, expression of the kauralexin enzymes, kaurene oxidase 2 (*Zm*KO2) and kauralexin reductase 2 (*Zm*KR2)[18] fail to significantly reduce the accumulation of ZA1 resulting from the expression of ZX3 and ZX6 (Supplementary Fig. 27). Similarly, expression of ZX9 has no impact on the accumulation of KB1 produced by the combination of *Zm*An2, *Zm*KSL2 and *Zm*CYP71Z18 (ZX6). As positive controls, in both cases, more terminal pathway-specific enzymes significantly reduced the accumulation of ZX and kauralexin precursors and resulted in the accumulation of late pathway products (Supplementary Fig. 27).

With an emphasis on ZXs and kauralexins, in which late pathway enzymes are now known[18], we present an integrated pathway model comprising three layers of interacting components: (1) a collection of sesquiterpene and diterpene synthases generating structurally diverse hydrocarbon olefin precursors that together (2) function as substrates for a family of catalytically promiscuous CYP71Z P450 enzymes, enabling partially overlapping pathway functions and diverse products that (3) are subsequently further decorated and diversified after reconnection with a final layer of pathway-specific enzymes (Supplementary Fig. 27). Collectively, our data support the hypotheses that a breadth of TPS-derived metabolites converges on a single CYP71Z node before again being expanded through pathway-specific downstream enzyme activities. Thus, maize defensive terpenoid metabolism seems to occur through an hourglass-shaped biosynthetic network rather than distinct individual pathways to produce a cocktail of oxidized antibiotics (Fig. 6a).

Fig. 5 | ZX-pathway activation occurs during the large-scale reprograming of fungal-induced defences. a, Biochemical defence activation on the basis of the relative amounts of major BXs, acidic terpenoids and flavonoids present—estimated from liquid chromatography coupled with MS (LC–MS) peak areas—in intact maize (var. Golden Queen) stem tissues (control (Con)) or those slit and treated with either H_2O (damaged (Dam)) or heat-killed *F. venenatum* hyphae (Fungus) aged 11 d, 25 d and 35 d and harvested 3 d later. Data are mean ± s.e.m. $n = 4$ biologically independent replicates. Within the plots, different letters (a and b) represent significant differences for the *F. venenatum* treatment; statistical analysis was performed using one-way ANOVA, $P < 0.05$; Tukey tests were used to correct for multiple comparisons, $P < 0.05$. **b**, Complete-linkage hierarchical clustering of 10,508 unique protein fold changes paired with mapping of $\log_2$-transformed RNA fold changes during a *F. venenatum* elicitation time course of 120 h in W22 stems using plants aged 38 d. The vertical lines correspond to individual gene IDs. Rows are organized by time point, data type and colours (blue, underexpressed; yellow, overexpressed). **c**, WGCNA of the proteomic and transcriptomic data from the W22 *F. venenatum* elicitation time course identified modules with distinct regulation patterns. Module 1 (4,787 gene IDs) contains highly cosuppressed gene–protein pairs, including early steps in BX biosynthesis, whereas module 3 (1,534 gene IDs) contains highly elicited coaccumulating gene–protein pairs, including the ZX biosynthetic pathway. The vertical axes indicate expression values relative to the mean expression across all of the time points. **d**, Heat maps of normalized protein fold changes in the W22 stem *F. venenatum* elicitation time course for BX, ZX and flavone pathways. The corresponding metabolite fold changes for representative BXs (2,4-dihydroxy-7-methoxy-1,4-benzoxazin-3-one glucoside (DIMBOA-glc); 2-hydroxy-4,7-dimethoxy-1,4-benzoxazin-3-one-Glc (HDMBOA-glc)) and flavone pathway metabolites (naringenin, apigenin) were analysed using LC–MS, whereas ZXs (ZA1 and ZB1) were analysed using GC–MS. PP, pyrophosphate. Coloured scale bars in **d** indicate the fold change of normalized protein. The definitions of B73 RefGen_V4 gene IDs and all abbreviations are provided in Supplementary Table 2.

Previous studies have indirectly linked β-macrocarpene synthases, ZX production and disease resistance[29,32–35]. To examine endogenous relationships, we generated *zx1 zx2 zx3* triple and *zx1 zx2 zx3 zx4* quadruple insertion- and deletion-based mutants using CRISPR–Cas9 gene editing (Supplementary Fig. 28). Ten days after stalk inoculation with *F. graminearum*, *zx1 zx2 zx3 zx4*

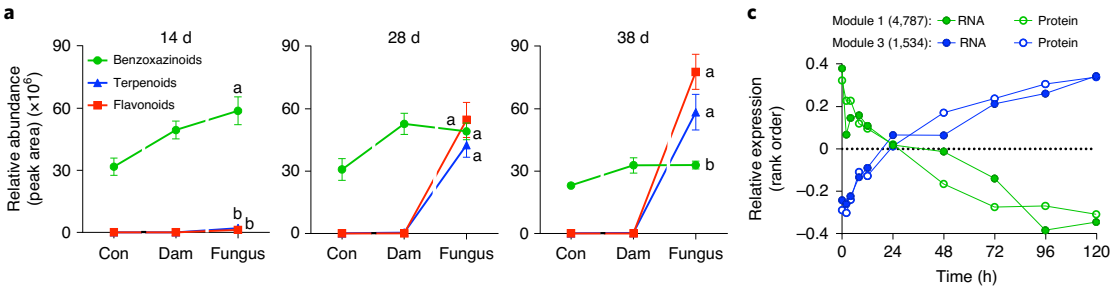

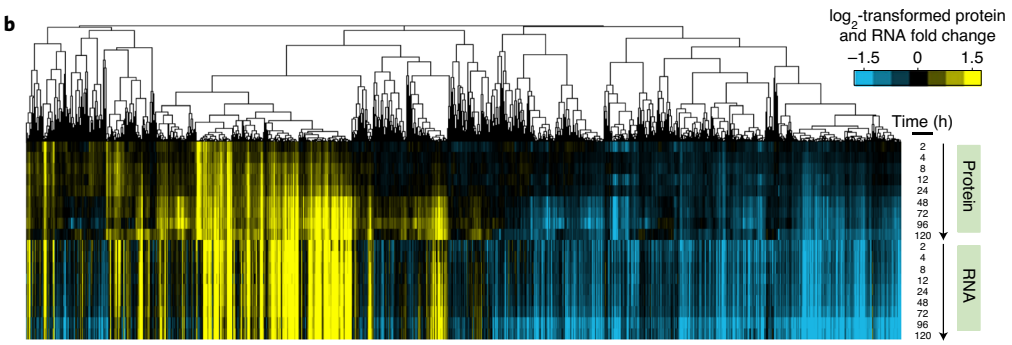

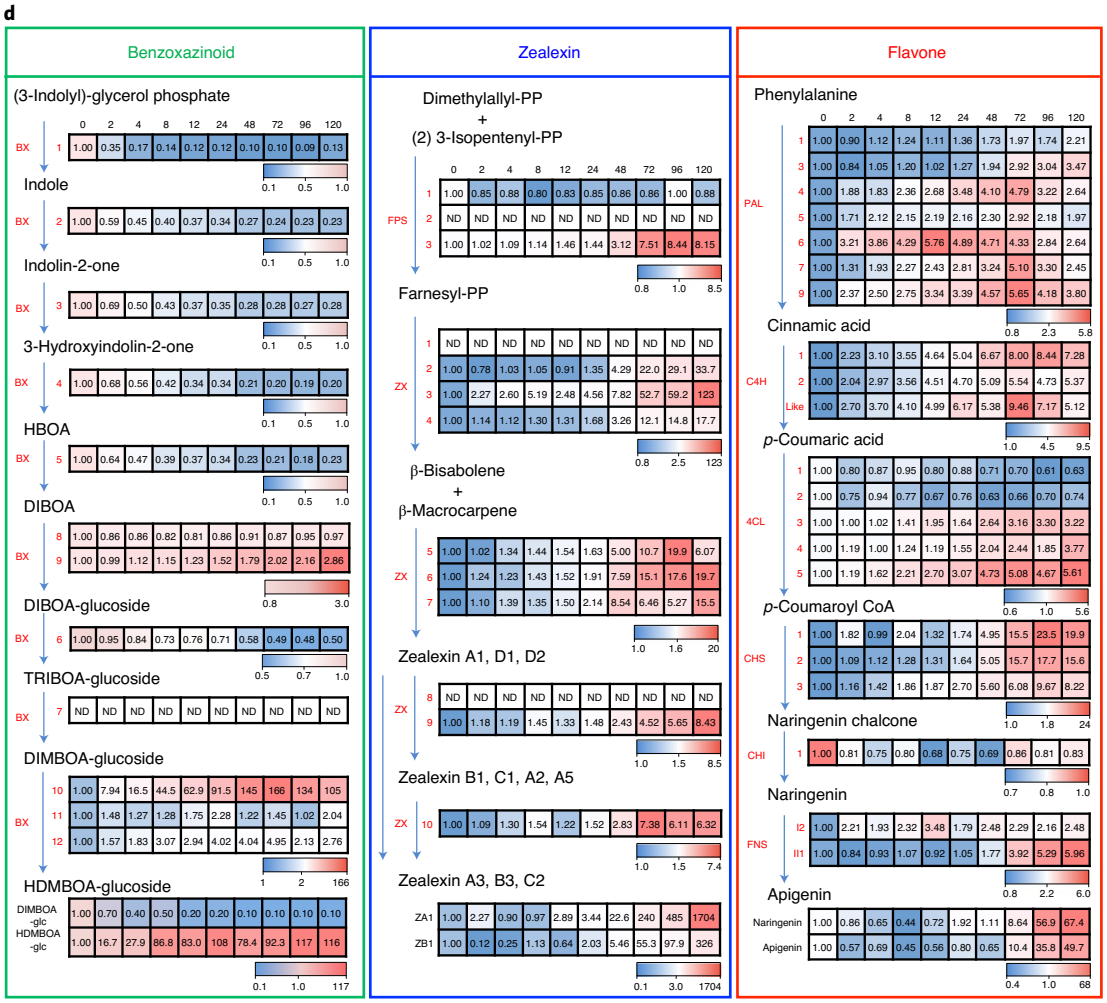

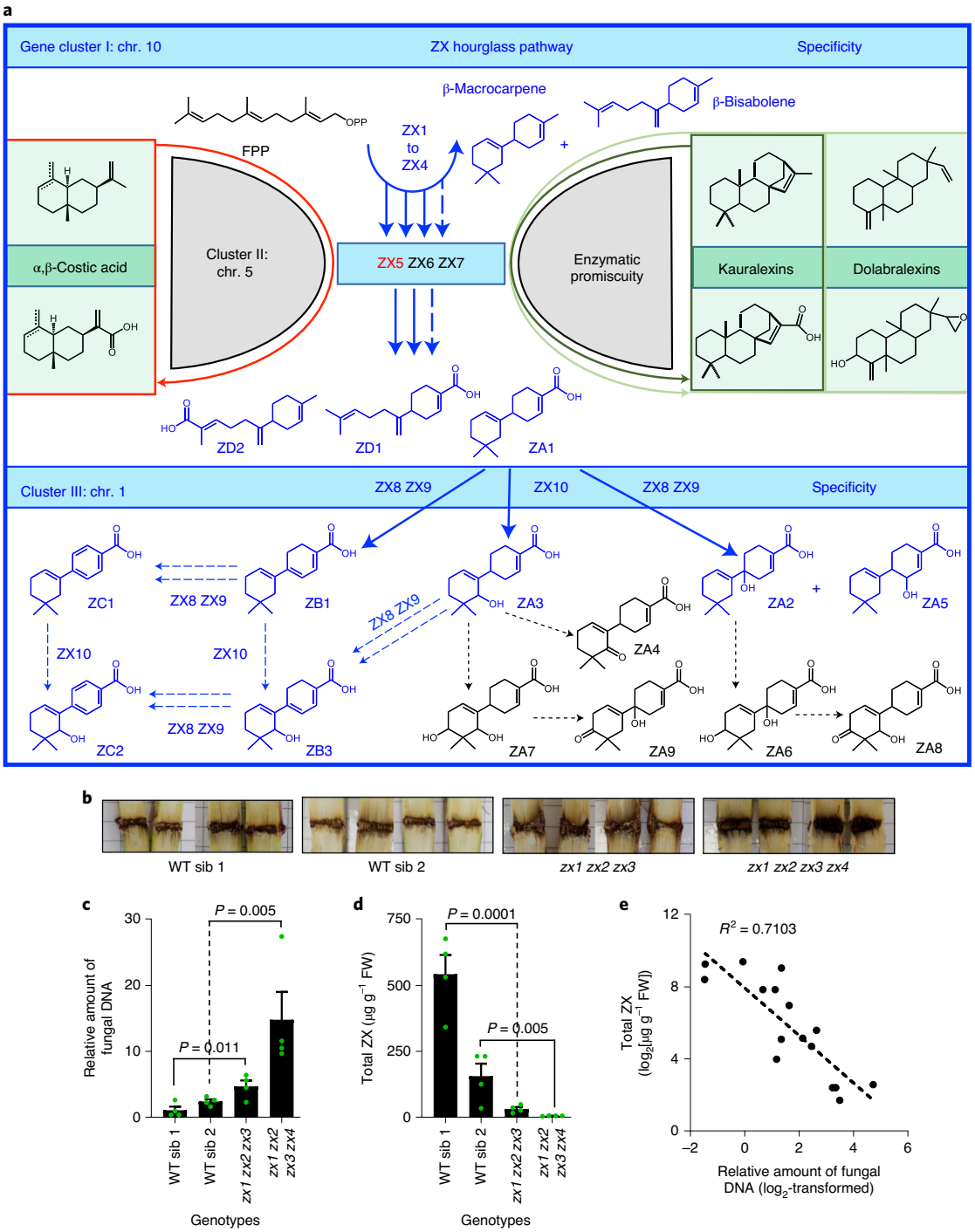

Fig. 6 | The maize ZX pathway is a biosynthetic hourglass with genetic redundancy and enzyme promiscuity that ensures the production of protective antibiotic cocktails. a, Schematic of enzyme activities encoded by *Zx* gene clusters I (*Zx1* to *Zx4*), II (*Zx5* to *Zx7*) and III (*Zx8* to *Zx10*), including interactions with additional pathways, such as kauralexins (dark green), dolabralexins (light green) and costic acids (red). Combined genomic, transcriptomic, proteomic, association mapping, enzyme coexpression studies and NMR-based structure elucidation support the genome-wide role of ZX1 to ZX10 in the production of 17 pathway products. The solid blue line arrows represent enzyme catalysis supported by genetics and in vivo expression studies. The dashed blue line arrows indicate demonstrated activities of gene cluster III that require enzyme feeding studies to clarify the predominant order of catalysis. The dashed black line arrows represent undefined enzyme activities. **b**, Representative disease levels in stems of CRISPR–Cas9-derived triple (*zx1zx2zx3*) and quadruple (*zx1zx2zx3zx4*) mutants and the respective wild-type siblings (WT sib), which were grown for 25 d and were stem-inoculated with *F. graminearum* (10 μl of 1.5×10^5 conidia per ml) for 10 d. Eight biological replicates were performed and showed similar results. **c**, The relative amount of fungal DNA in triple (*zx1zx2zx3*) and quadruple (*zx1zx2zx3zx4*) mutants and the respective wild-type siblings. RT–qPCR was used to determine the ratio of fungal DNA (Fg*Tri6*) to maize DNA (Zm*RPL17*) in stems 10 d after inoculation. **d**, Total ZX (μg g^{-1} fresh weight (FW)) present in triple (*zx1zx2zx3*) and quadruple (*zx1zx2zx3zx4*) mutants and the respective wild-type siblings as measured using GC–MS. **e**, $\log_2$-transformed correlation of endogenous ZX with the relative amount of fungal DNA in triple (*zx1zx2zx3*) and quadruple (*zx1zx2zx3zx4*) mutants and the respective wild-type siblings. For **c** and **d**, data are mean ± s.e.m. $n = 4$ biologically independent replicates. *P* values were determined using Student's *t*-tests, two-tailed distribution, equal variance.

mutant plants displayed visible (Fig. 6b) and quantitative increases in disease susceptibility, as estimated by the relative amount of fungal DNA (Fig. 6c). In contrast to wild-type plants and *zx1 zx2 zx3* plants containing a single β-macrocarpene synthase, *zx1 zx2 zx3 zx4* mutants consistently displayed a lack of detectable ZXs after inoculation with *F. graminearum* (Fig. 6d), yet were not impaired in kauralexin production (Supplementary Fig. 29). Across all samples, ZX production was negatively correlated ($R^2 = 0.71$) with *F. graminearum* DNA levels (Fig. 6e). Initially derived from HiII—a complex genetic background containing B73 and A188—wild-type siblings for zx1 zx2 zx3 and *zx1 zx2 zx3 zx4* mutants displayed differential biosynthetic abilities for ZX accumulation, emphasizing the importance of multiple controls (Fig. 6c,d). Enhanced disease susceptibility to Stewart's wilt, which is caused by the xylem-dwelling bacteria *Pantoea stewartii*, was similarly observed in *zx1 zx2 zx3 zx4* mutants (Supplementary Fig. 30), demonstrating protective roles against diverse pathogens. Suppression of root ZX production in *zx1 zx2 zx3* and *zx1 zx2 zx3 zx4* mutants (Supplementary Fig. 31) also significantly altered the root bacterial microbiome associated with plants grown in field soil, lowering evenness and altering the abundances of particular taxa (Supplementary Fig. 32 and Supplementary Table 13). Collectively, the ZX pathway and complex array of resulting antibiotics has a significant role in maize interactions with microorganisms.

Discussion

An understanding of the genetic, biosynthetic and regulatory machinery that controls innate immunity is essential for optimizing biochemical defences and crop resistance traits. For insights into maize disease resistance, we leveraged multi-omic approaches to elucidate hidden biochemical layers of immunity. Here we characterized ten genes that are present in three distinct gene clusters that ensure the production of 17 ZX pathway metabolites with collective antibiotic action (Fig. 6a, Supplementary Table 2, and Supplementary Figs. 1, 2 and 21). Our data collectively support the existence of a biosynthetic hourglass pathway (Fig. 6a) whereby maize antibiotics production relies on enzymes encoded by three Zm*CYP71Z*-family genes (*Zx5* to *Zx7*) on chromosome 5 that contribute to multiple distinct families of sesquiterpenoids and diterpenoids[18,30]. Maize antibiotic biosynthesis seems to be highly interconnected, and provides a model for how complex combinatorial blends are biosynthesized, contributing to immunity against diverse microorganisms.

Association mapping efforts to uncover genetic loci responsible for quantitative resistance to diverse maize pathogens commonly result in the discovery of multiple loci with comparatively small effects that explain 1–3% of trait variation[21,53,54]. ZX product complexity, pathway redundancy and overall resiliency to mutations are consistent with multiple disease-resistance quantitative trait loci that are commonly too small to be detected individually[22]. In contrast to qualitative resistance genes—such as wall-associated kinase (Zm*WAK*), which protects against head smut (*Sporisorium reilianum*)[55]—ZX biosynthesis as a trait is not controlled by a single Mendelian locus. At each of the three *Zx* gene clusters, pan-genome expression, sequence-level or gene-copy-level variation exists, which can impact individual pathway enzymes; however, gene-cluster redundancies ensure ZX biosynthesis.

Zx gene cluster I, which is encoded on chromosome 10, most commonly contains four tandem duplicate β-bisabolene/β-macrocarpene synthase genes, termed *Zx1* to *Zx4*. Comparative coexpression in *N. benthamiana* was used to prove pathway products (Fig. 1) and to understand the catalytic differences in ZX1 controlled by a single SNP common among inbred lines (Supplementary Fig. 6 and Supplementary Table 5). With genetic variation driving exonic changes and observed differences in relative expression, varying functional copies of *Zx1* to *Zx4* are commonly maintained in the maize pan-genome with inbred-specific patterns (Fig. 1a–i, Supplementary Fig. 7 and Supplementary Table 7). ZX pathway redundancy contrasts with both the BX and kauralexin pathways, for which single gene mutations in indole-3-glycerol phosphate lyase (*benzoxazinless1*, *bx1*) and kaurene synthase-like 2 (Zm*ksl2*) can reduce pathway metabolites to 1% of the wild-type levels and impair biotic stress resistance[5,18,56]. ZX-pathway resiliency to single-gene mutations, coupled with reduced pathogen resistance in *zx1 zx2 zx3 zx4* quadruple mutants, supports the hypothesis that maize relies on ZXs as key biochemical defences.

To generate acidic non-volatile antibiotics, *Zx* gene cluster II on chromosome 5 contains three neighbouring duplicated *CYP71Z* genes (*Zx5* to *Zx7*) that each display variable coexpression with *Zx1* to *Zx4* (Fig. 2a and Supplementary Fig. 27) and drive the production of ZA1, ZD1 and ZD2 (Fig. 2d,e). Previously associated with the synthesis of kauralexins, dolabralexins and ZA1, ZX6 and ZX7 contribute to a powerful in vivo system for combinatorial chemistry[18,30]. We now demonstrate that ZX5 also acts on broader sesquiterpene olefins, including the Zm*TPS21* product β-selinene to produce β-costic acid. However, ZX5 lacks appreciable kauralexin biosynthetic activity (Supplementary Fig. 14), highlighting specific differences in the product-diversifying roles of enzymes contained in *Zx* gene cluster II. Syntenic to *Zx5*, the closely related *Sorghum* gene Sb*CYP71Z19* encodes an enzyme that similarly generates acids from β-selinene, β-bisabolene and β-macrocarpene, indicating that the biosynthetic ability of related genes to oxidize diverse terpenoid precursors existed in a common ancestor of maize and *Sorghum* (Supplementary Figs. 14 and 15). Our present systematic analyses of gene cluster II also uncovered the presence of only two related Zm*CYP71Z* genes in teosinte—which, together with synteny and activity in Sb*CYP71Z19*—provides new insights into the origin of ZXs (Supplementary Figs. 9, 11, 14 and 15). The high degree of coregulation between the sum expression of *Zx1* to *Zx4* with *Zx5*, and comparative sesquiterpene substrate specificity are consistent with an important role for ZX5 in ZX biosynthesis while maintaining the flexible resiliency of gene cluster II to deleterious mutation (Fig. 2a,b and Supplementary Figs. 11 and 14).

Genetic fine-mapping on chromosome 1 identified *Zx* gene cluster III, which unexpectedly revealed three related CYP81A-family P450s. Although the CYP81 subfamily have established roles in the specialized metabolism surrounding glucosinolate, isoflavonoid, lignan and xanthone biosynthesis, none have previously been demonstrated to utilize terpenoid substrates (Supplementary Fig. 23 and Supplementary Table 3). ZX8 and ZX9 are functionally redundant, acting on ZA1 to produce four oxidized products, namely ZA2, ZA5, ZB1 and ZC1 (Fig. 4a,b). Successive rounds of oxidation at the C6 position probably yield the observed C1–C6 desaturation in ZB1 (ref. [57]). *Zx10* represents the sole non-redundant pathway gene, encoding *Zm*CYP81A39, which is responsible for ZX C8 oxidation to an alcohol and the combined variants ZA3, ZB3 and ZC2 (Fig. 4a,b). Additional ZXs, namely ZA6 to ZA9, displaying C10 oxidations to alcohols and ketones, were also identified in maize tissues; however, the final enzymes that are responsible remain unknown. Collectively ZX1 to ZX10 account for the production of 12 out of the 17 identified ZX pathway precursors and end products (Fig. 6a). As a major product of ZX1 to ZX9 action, ZB1 exhibits significant antifungal activity at 25 μg ml^{-1} against two key *Fusarium* pathogens of maize (Supplementary Fig. 21).

ZX biosynthesis is a highly coregulated pathway, fully contained in WGCNA module 3 that includes 1,534 transcript–protein pairs that are enriched for predominant GO terms 'response to stimulus' and 'secondary metabolic processes' (Fig. 5c and Supplementary Tables 10 and 11). Beyond terpenoids, phenylpropanoid defences, including naringenin, chalcone, apigenin and apigenin 7-*O*-methyl ether, are known to accumulate in maize after anthracnose stalk rot (*Colletotrichum graminicola*) infection and reduce fungal

growth[51]. Our current research demonstrates that fungal-elicited flavonoid-pathway activation in maize is highly coordinated with terpenoid defences (Fig. 5a,d). Multi-omic analyses place ZX biosynthesis in the context of massive reorganization of the transcriptome and proteome, including a fivefold suppression of early BX biosynthetic enzymes (BX1 to BX5; Fig. 5d) and, more generally, an enrichment in GO terms that define processes surrounding 'DNA/RNA metabolism' in module 1 (Fig. 5c and Supplementary Tables 10 and 11). Together, our experiments address a fifteen-year-old hypothesis that sesquiterpenoids mediate maize disease resistance[32], consider ZXs in the context of multiple biochemical defence pathways and place ZXs among predominant antibiotics that contribute to defence (Figs. 5d and 6a–e).

Independent of genetic mechanisms pursued, the leveraged application of durable multiple-disease-resistance traits is a key goal in crop protection[22]. Efforts in *Sorghum* have resulted in the identification of complete defence pathways, defined enzyme organization in biosynthetic metabolons and enabled the relocation of pathways to specific organelles in heterologous plants[58,59]. Capturing the full breadth of resistance traits provided by complex pathways requires an understanding of interconnections and biosynthetic nodes. To demonstrate the comparative importance of individual maize antibiotics pathways and other defence mechanisms, a combinatorial series of pathway knockouts would be needed for *zx1 zx2 zx3 zx4*, Zm*tps21* (ref. [28]), Zm*ksl2* (ref. [18]), Zm*ksl4* (ref. [30]) and established resistance genes of interest[60] in a single inbred line for diverse field trials. In each terpenoid pathway, evidence supports roles in resistance to *Fusarium* spp.[18,28,30]; however, assignments of relative importance between pathways are not presently possible. While speculative, gene duplications throughout the ZX biosynthetic pathway suggest additional selection pressures and protective roles[16]. Uncoupling pathways at different biosynthetic nodes presents a challenge given the evidence for ZX biosynthetic interactions with multiple terpenoid pathways mediated by promiscuous *Zm*CYP71Z enzymes. Although the full transfer of maize terpenoid antibiotic defences to a non-native crop model would require a series of pathway genes, leveraging single-gene transfers and knowledge of enzyme promiscuity with existing modular pathways has recently provided enhanced levels of innate immunity in rice against fungal pathogens[36].

Pathogen-elicited terpenoid antibiotics have been studied in crops for more than 40 years and led to the discovery of TPS-mediated plant defences[16,61,62]. Despite a massive growth of comparative -omics, delineating clear connections between genotypes, chemotypes and phenotypes has remained a challenge owing to genetic redundancies and enzyme promiscuity. Our use of association analyses paired with transcriptional coregulation patterns, combinatorial biochemical studies and targeted mutant analyses using CRISPR–Cas9 collectively provides powerful tools to narrow and interrogate the metabolic pathways that control plant innate immunity. Heterologous enzyme coexpression studies efficiently define candidate gene functions, impact of genomic variation, promiscuity, redundancy and endogenous pathway interactions leading to antibiotic complexity. Comprehensive proteomics confirms the existence of endogenous translation products and gives a more complete context to the regulation of multiple pathways that are known to, or suspected to, impact defence phenotypes. Our present elucidation of highly interconnected antibiotic pathways illuminates complex combinatorial strengths in the genus *Zea*, which can now be considered in breeding and additional pathway engineering approaches to effectively enhance disease resistance in crops[36].

Methods

Plant and fungal materials. Maize seeds for the IBM RILs[43] and the Goodman diversity panel[39] were provided by G. Jander (Boyce Thompson Institute) and P. Balint-Kurti (US Department of Agriculture, Agricultural Research Service (USDA-ARS)). Nested association mapping[44] parental line seeds and B73 × Mo17 NILs were obtained from the Maize Genetics Cooperation Stock Center. A list of all of the maize lines used for genetic mapping efforts is provided in Supplementary Table 14. *Zea perennis* (Ames 21874), *Zea diploperennis* (PI 462368), *Zea luxurians* (PI 422162), *Zea mays parviglumis* (PI 384069) and *Z. m. mexicana* (Ames 21851) were provided by the USDA-ARS (North Central Regional Plant Introduction Station). Maize inbred lines that were used for replicated elicitation experiments were germinated in Metro-Mix 200 (Sun Gro Horticulture Distribution) supplemented with 14-14-14 Osmocote (Scotts Miracle-Gro) and grown in a greenhouse as previously described[28]. Fungal cultures of *F. graminearum* (NRRL 31084), *F. verticillioides* (NRRL 20956), *A. flavus* (NRRL 3357) and SLB (*C. heterostrophus*) were grown on V8 agar for 12 d before the spores were quantified and used[29]. Heat-killed *F. venenatum* (strain PTA-2684) hyphae were commercially obtained (Monde Nissin) and used as a uniform non-infectious elicitor to avoid complexities in diverse germplasm responses, which are likely to occur across a spectrum of susceptible and resistant interactions with live pathogens. In total, maize experiments utilized multiple pathogens, including *Fusarium*, heat-killed *Fusarium*, *Aspergillus, Cochliobolus, Pantoea* and combined microbial complexities associated with field soil to address a range of interactions in which the ZX pathway is present and is likely to be activated.

Maize stem challenge with heat-killed *Fusarium* and live fungi. Using a scalpel, plants (aged 35 d) were slit in the centre, spanning both sides of the stem, to create a 10 cm longitudinal incision. The incision wounded the upper nodes, internodes and the most basal portion of unexpanded leaves. For replicated ($n = 3$–4) 36 h experiments using B73 and Mo17, the ten-point ($n = 1$) 0–120 h time course with W22 (ref. [18]) and the three-day treatment of the Goodman diversity panel, approximately 500 µl of commercial heat-killed *F. venenatum* hyphae was introduced into each slit stem, and then the site was sealed with clear plastic packing tape to minimize desiccation of the treated tissues. B73 and Mo17 experiments included parallel wound control plants lacking fungal hyphae treatment. For the quantification of ZX diversity after *C. heterostrophus* inoculation, maize (*Z. mays* var. Golden Queen) plants were wounded as described above and treated with either 100 µl of H_2O or an aqueous *C. heterostrophus* spore (1×10^7 ml^{-1}) suspension. Damage controls and *C. heterostrophus*-treated plants were harvested each day for three consecutive days. For the stalk-rot resistance assay, a hole (diameter, 1 mm) was created through the second aboveground node in the stalk of plants (aged 35 d) and inoculated with either 10 µl of H_2O or 10 µl of a *F. graminearum*-spore (1.5×10^5 ml^{-1}) suspension. After 10 d, stems were longitudinally slit with a scalpel, photographed and harvested using pool of two individual plants for each of the four final harvested replicates. Within each experiment, treated maize stem tissues were harvested into liquid N_2 at specific time points as indicated.

***Pantoea stewartii* resistance assay.** *P. stewartii* ssp. *stewartii* strain DC283 harbouring the plasmid pHC60 encoding GFP^{S65T} (DC283-GFP; nalR and tetR) was used as described previously[63]. Nalidixic acid (30 µg ml^{-1}) and tetracycline (20 µg ml^{-1}) were used for selection of DC283-GFP when grown in Luria-Bertani (LB) agar and LB broth at 28 °C. Bacteria were subcultured by diluting 1:10 into 10 ml final volume with antibiotics and grown to an optical density at 600 nm (OD_{600}) of 0.7. Bacteria were harvested by centrifuging at 2,800*g* for 10 min and resuspended in PBS supplemented with 0.01% Tween-20 (PBST buffer) three times. Final bacterial OD was adjusted to an OD_{600} of 0.2 and used for infiltration. Maize seedlings (aged 12 d) were punctured with a needle (diameter, 1 mm) in the internode between aboveground node 1 and node 2 and infiltrated with 10 µl PBS buffer (mock) or 10 µl *P. stewartii*. Plants were evaluated after 5 d for bacterial growth by GFP quantification and 16 d after infection for visual symptoms by counting the number of dying leaves per plant due to bacterial wilting. Progression of *P. stewartii*-GFP bacteria in veins was visualized by illumination with blue light using a Dark Reader Spot Lamp (DRSL; Clare Chemical Research) as previously described[64]. To quantify *P. stewartii*-GFP, total protein from infected leaf tissue was extracted in PBST buffer. GFP fluorescence intensity was measured using a Synergy H1 Multi-Mode microplate reader (BioTek) equipped with a green filter cube (excitation 485/20 nm, emission 528/20 nm) using total-protein extract from mock-inoculated plants as a blank[64]. GFP fluorescence intensity was normalized to the highest fluorescence value and is shown as relative fluorescence units (RFU). For each extraction, two technical replicates were averaged and used to calculate RFU.

RNA-seq analyses of fungal-elicited genes. To examine B73 and Mo17 defence transcript changes after elicitation with heat-killed *Fusarium* hyphae, total RNA was isolated using the NucleoSpin RNA Plant Kit (Takara Bio) according to the manufacturer's protocol. RNA quality was assessed on the basis of RNA integrity number using an Agilent Bioanalyzer. 3′ RNA-seq library construction and sequencing were performed at Cornell University's Genomics Facility, Institute of Biotechnology (Ithaca; http://www.biotech.cornell.edu/brc/genomics-facility/services). Approximately 500 ng of total RNA was used to construct the 3′ RNA-seq libraries using the QuantSeq 3′ mRNA-seq Library Prep Kit FWD (Lexogen) according to the manufacturer's instructions. All of the libraries, each with their own unique adapter sequences, were pooled together and sequenced in one lane

of an Illumina NextSeq 500 to generate 90-bp single-end reads. Trimmomatic (v.0.39) was used to remove Illumina TruSeq adapter sequences and trim the first 12 bp (ref. [65]). Trimmed reads were aligned to the maize B73 V4 reference genome (ensemble 4.44) using Hisat2 (v.2.0.0)[66] and sorted using Sambamba (v.0.6.8)[67]. Raw mapped reads were quantified using featureCounts (v.1.6.4)[68]. Counts per million were processed in R with DESeq2 to generate normalized read counts using the default method and transformation of the normalized counts was performed using the rlog transformation method[69].

For the analyses of W22 tissues, RNA-seq library construction and sequencing were performed by Novogene. The mRNA was first enriched from total RNA using oligo (dT) magnetic beads and then fragmented randomly into short sequences followed by first-strand cDNA synthesis with random hexamer-primed reverse transcription. Second-strand cDNA synthesis was performed by nick-translation using RNase H and DNA polymerase I. After adapter end repair and ligation, cDNA was amplified using PCR and purified to create the final cDNA library. cDNA concentration was quantified using a Qubit (v.2.0) fluorometer (Life Technologies) and then diluted to 1 ng μl^{-1}, before assessing insert size using an Agilent Bioanalyzer 2100. Library preparations were sequenced using an Illumina platform and paired-end reads were obtained. Image analysis and base calling were performed using the standard Illumina pipeline. Raw reads were filtered to remove reads containing adapters or reads of low quality. Qualified reads were then aligned to *Z. mays* AGPv4 reference genome using TopHat (v.2.0.12)[70]. Gene expression values, calculated as fragments per kilobase per million reads, were analysed using HTSeq (v.0.6.1)[71].

Statistical analyses. Statistical analyses were conducted using JMP Pro v.13.0 (SAS Institute) and Prism v.8.0 (GraphPad). One-way ANOVA was performed to evaluate statistical differences. Tukey tests were used to correct for multiple comparisons between control and treatment groups. Student's unpaired two-tailed *t*-tests were conducted for pairwise comparisons. $P < 0.05$ were considered to be statistically significant.

Further information on the research methods is available in the Supplementary Information.

Reporting Summary. Further information on research design is available in the Nature Research Reporting Summary linked to this article.

Data availability

Publicly available datasets used in the study include the National Center for Biotechnology Information (NCBI) Sequence Read Archive project ID SRP115041 and the MaizeGDB BLAST database (https://maizegdb.org/popcorn/main/index.php). Raw read sequences have been deposited at the NCBI Gene Expression Omnibus under accession numbers GSE138961 and GSE138962. Raw sequence data from the root microbiome are available at NCBI BioProject under accession number PRJNA580260. Raw proteomic mass spectra have been deposited at the Mass Spectrometry Interactive Virtual Environment repository (ftp://massive.ucsd.edu/MSV000084285). Maize-related germplasm used in this research have been previously described[27,39,43–45,72,73] and can be obtained from US Department of Agriculture Germplasm Resources Information Network (https://www.ars-grin.gov) and the Maize Genetics Cooperation Stock Center (http://maizecoop.cropsci.uiuc.edu). Where possible, gene identifiers used throughout the manuscript were in reference to B73 RefGen_v4 (https://www.maizegdb.org/genome/assembly/Zm-B73-REFERENCE-GRAMENE-4.0), which was used as a foundation for the study. All data are available from the corresponding author on request.

Code availability

For the gene-duplication date estimations, scripts to perform translations, alignments and backtranslations as well as data files and BEAST control files have been deposited at GitHub (https://github.com/TomJKono/Zealexin_Dating).

Received: 16 March 2020; Accepted: 11 September 2020;
Published online: 26 October 2020

References

1. Ritchie, H. & Roser, M. Land use. *Our World in Data* https://ourworldindata.org/land-use (2020).
2. Evenson, R. E. & Gollin, D. Assessing the impact of the green revolution, 1960 to 2000. *Science* **300**, 758–762 (2003).
3. Cartwright, D., Langcake, P., Pryce, R. J., Leworthy, D. P. & Ride, J. P. Chemical activation of host defence mechanisms as a basis for crop protection. *Nature* **267**, 511–513 (1977).
4. Snyder, B. A. & Nicholson, R. L. Synthesis of phytoalexins in *Sorghum* as a site-specific response to fungal ingress. *Science* **248**, 1637–1639 (1990).
5. Frey, M. et al. Analysis of a chemical plant defense mechanism in grasses. *Science* **277**, 696–699 (1997).
6. Goswami, R. S. & Kistler, H. C. Heading for disaster: *Fusarium graminearum* on cereal crops. *Mol. Plant Pathol.* **5**, 515–525 (2004).
7. Mueller, D. et al. Corn yield loss estimates due to diseases in the United States and Ontario, Canada from 2012 to 2015. *Plant Health Prog.* **17**, 211–222 (2016).
8. Genetics for a warming world. *Nat. Genet.* **51**, 1195–1195 (2019).
9. Dixon, R. A. Natural products and plant disease resistance. *Nature* **411**, 843–847 (2001).
10. Jones, J. D. G. & Dangl, J. L. The plant immune system. *Nature* **444**, 323–329 (2006).
11. van Loon, L. C., Rep, M. & Pieterse, C. M. J. Significance of inducible defense related proteins in infected plants. *Annu. Rev. Phytopathol.* **44**, 135–162 (2006).
12. Moghe, G. D. & Kruse, L. H. The study of plant specialized metabolism: challenges and prospects in the genomics era. *Am. J. Bot.* **105**, 959–962 (2018).
13. Wouters, F. C., Blanchette, B., Gershenzon, J. & Vassao, D. G. Plant defense and herbivore counter-defense: benzoxazinoids and insect herbivores. *Phytochem. Rev.* **15**, 1127–1151 (2016).
14. Meihls, L. N. et al. Natural variation in maize aphid resistance is associated with 2,4-dihydroxy-7-methoxy-1,4-benzoxazin-3-one glucoside methyltransferase activity. *Plant Cell* **25**, 2341–2355 (2013).
15. Fraenkel, G. S. The raison d'etre of secondary plant substances; these odd chemicals arose as a means of protecting plants from insects and now guide insects to food. *Science* **129**, 1466–1470 (1959).
16. Schmelz, E. A. et al. Biosynthesis, elicitation and roles of monocot terpenoid phytoalexins. *Plant J.* **79**, 659–678 (2014).
17. Vaughan, M. M. et al. Accumulation of terpenoid phytoalexins in maize roots is associated with drought tolerance. *Plant Cell Environ.* **38**, 2195–2207 (2015).
18. Ding, Y. et al. Multiple genes recruited from hormone pathways partition maize diterpenoid defences. *Nat. Plants* **10**, 1043–1056 (2019).
19. Casas, M. I. et al. Identification and characterization of maize salmon silks genes involved in insecticidal maysin biosynthesis. *Plant Cell* **28**, 1297–1309 (2016).
20. Degenhardt, J. Indirect defense responses to herbivory in grasses. *Plant Physiol.* **149**, 96–102 (2009).
21. Zila, C. T., Samayoa, L. F., Santiago, R., Butron, A. & Holland, J. B. A genome-wide association study reveals genes associated with *Fusarium* ear rot resistance in a maize core diversity panel. *G3* **3**, 2095–2104 (2013).
22. Wiesner-Hanks, T. & Nelson, R. Multiple disease resistance in plants. *Annu Rev. Phytopathol.* **54**, 229–252 (2016).
23. Stagnati, L. et al. A genome wide association study reveals markers and genes associated with resistance to *Fusarium verticillioides* infection of seedlings in a maize diversity panel. *G3* **9**, 571–579 (2019).
24. Banerjee, A. & Hamberger, B. P450s controlling metabolic bifurcations in plant terpene specialized metabolism. *Phytochem. Rev.* **17**, 81–111 (2018).
25. Karunanithi, P. S. & Zerbe, P. Terpene synthases as metabolic gatekeepers in the evolution of plant terpenoid chemical diversity. *Front. Plant Sci.* **10**, 1166 (2019).
26. Block, A. K., Vaughan, M. M., Schmelz, E. A. & Christensen, S. A. Biosynthesis and function of terpenoid defense compounds in maize (*Zea mays*). *Planta* **249**, 21–30 (2019).
27. Springer, N. M. et al. The maize W22 genome provides a foundation for functional genomics and transposon biology. *Nat. Genet.* **50**, 1282–1288 (2018).
28. Ding, Y. Z. et al. Selinene volatiles are essential precursors for maize defense promoting fungal pathogen resistance. *Plant Physiol.* **175**, 1455–1468 (2017).
29. Huffaker, A. et al. Novel acidic sesquiterpenoids constitute a dominant class of pathogen-induced phytoalexins in maize. *Plant Physiol.* **156**, 2082–2097 (2011).
30. Mafu, S. et al. Discovery, biosynthesis and stress-related accumulation of dolabradiene-derived defenses in maize. *Plant Physiol.* **176**, 2677–2690 (2018).
31. Mao, H., Liu, J., Ren, F., Peters, R. J. & Wang, Q. Characterization of CYP71Z18 indicates a role in maize zealexin biosynthesis. *Phytochemistry* **121**, 4–10 (2016).
32. Basse, C. W. Dissecting defense-related and developmental transcriptional responses of maize during *Ustilago maydis* infection and subsequent tumor formation. *Plant Physiol.* **138**, 1774–1784 (2005).
33. Kollner, T. G. et al. Protonation of a neutral (*S*)-β-bisabolene intermediate is involved in (*S*)-β-macrocarpene formation by the maize sesquiterpene synthases TPS6 and TPS11. *J. Biol. Chem.* **283**, 20779–20788 (2008).
34. Christensen, S. A. et al. Fungal and herbivore elicitation of the novel maize sesquiterpenoid, zealexin A4, is attenuated by elevated CO_2. *Planta* **247**, 863–873 (2018).
35. van der Linde, K., Kastner, C., Kumlehn, J., Kahmann, R. & Doehlemann, G. Systemic virus-induced gene silencing allows functional characterization of maize genes during biotrophic interaction with *Ustilago maydis*. *N. Phytol.* **189**, 471–483 (2011).
36. Shen, Q. et al. CYP71Z18 overexpression confers elevated blast resistance in transgenic rice. *Plant Mol. Biol.* **100**, 579–589 (2019).

37. Medema, M. H. et al. Minimum information about a biosynthetic gene cluster. *Nat. Chem. Biol.* **11**, 625–631 (2015).
38. Kersten, R. D., Diedrich, J. K., Yates, J. R. 3rd & Noel, J. P. Mechanism-based post-translational modification and inactivation in terpene synthases. *ACS Chem. Biol.* **10**, 2501–2511 (2015).
39. Flint-Garcia, S. A. et al. Maize association population: a high-resolution platform for quantitative trait locus dissection. *Plant J.* **44**, 1054–1064 (2005).
40. Kremling, K. A. G. et al. Dysregulation of expression correlates with rare-allele burden and fitness loss in maize. *Nature* **555**, 520–523 (2018).
41. Jones, C. G. et al. Sandalwood fragrance biosynthesis involves sesquiterpene synthases of both the terpene synthase (TPS)-a and TPS-b subfamilies, including santalene synthases. *J. Biol. Chem.* **286**, 17445–17454 (2011).
42. Swigonova, Z. et al. Close split of *Sorghum* and maize genome progenitors. *Genome Res.* **14**, 1916–1923 (2004).
43. Lee, M. et al. Expanding the genetic map of maize with the intermated B73 x Mo17 (IBM) population. *Plant Mol. Biol.* **48**, 453–461 (2002).
44. McMullen, M. D. et al. Genetic properties of the maize nested association mapping population. *Science* **325**, 737–740 (2009).
45. Eichten, S. R. et al. B73-Mo17 near-isogenic lines demonstrate dispersed structural variation in maize. *Plant Physiol.* **156**, 1679–1690 (2011).
46. Suzuki, R., Iijima, M., Okada, Y. & Okuyama, T. Chemical constituents of the style of *Zea mays* L. with glycation inhibitory activity. *Chem. Pharm. Bull.* **55**, 153–155 (2007).
47. Ahmad, S. et al. Benzoxazinoid metabolites regulate innate immunity against aphids and fungi in maize. *Plant Physiol.* **157**, 317–327 (2011).
48. Smissman, E. E., Lapidus, J. B. & Beck, S. D. Corn plant resistance factor. *J. Org. Chem.* **22**, 220–220 (1957).
49. Pollastri, S. & Tattini, M. Flavonols: old compounds for old roles. *Ann. Bot.* **108**, 1225–1233 (2011).
50. Lange, B. M. The evolution of plant secretory structures and emergence of terpenoid chemical diversity. *Annu. Rev. Plant Biol.* **66**, 139–159 (2015).
51. Balmer, D., de Papajewski, D. V., Planchamp, C., Glauser, G. & Mauch-Mani, B. Induced resistance in maize is based on organ-specific defence responses. *Plant J.* **74**, 213–225 (2013).
52. Yang, F. et al. A maize gene regulatory network for phenolic metabolism. *Mol. Plant* **10**, 498–515 (2017).
53. Benson, J. M., Poland, J. A., Benson, B. M., Stromberg, E. L. & Nelson, R. J. Resistance to gray leaf spot of maize: genetic architecture and mechanisms elucidated through nested association mapping and near-isogenic line analysis. *PLoS Genet.* **11**, e1005045 (2015).
54. Kump, K. L. et al. Genome-wide association study of quantitative resistance to southern leaf blight in the maize nested association mapping population. *Nat. Genet.* **43**, 163–168 (2011).
55. Zuo, W. et al. A maize wall-associated kinase confers quantitative resistance to head smut. *Nat. Genet.* **47**, 151–157 (2015).
56. Hamilton, R. H. A corn mutant deficient in 2,4-dihydroxy-7-methoxy-1,4-benzoxazin-3-one with an altered tolerance of atrazine. *Weeds* **12**, 27–30 (1964).
57. Meunier, B., de Visser, S. P. & Shaik, S. Mechanism of oxidation reactions catalyzed by cytochrome P450 enzymes. *Chem. Rev.* **104**, 3947–3980 (2004).
58. Henriques de Jesus, M. P. R. et al. Tat proteins as novel thylakoid membrane anchors organize a biosynthetic pathway in chloroplasts and increase product yield 5-fold. *Metab. Eng.* **44**, 108–116 (2017).
59. Laursen, T. et al. Characterization of a dynamic metabolon producing the defense compound dhurrin in *Sorghum*. *Science* **354**, 890–893 (2016).
60. Nelson, R., Wiesner-Hanks, T., Wisser, R. & Balint-Kurti, P. Navigating complexity to breed disease-resistant crops. *Nat. Rev. Genet.* **19**, 21–33 (2018).
61. Chappell, J. & Hahlbrock, K. Transcription of plant defense genes in response to UV-light or fungal elicitor. *Nature* **311**, 76–78 (1984).
62. Facchini, P. J. & Chappell, J. Gene family for an elicitor-induced sesquiterpene cyclase in tobacco. *Proc. Natl Acad. Sci. USA* **89**, 11088–11092 (1992).
63. Koutsoudis, M. D., Tsaltas, D., Minogue, T. D. & von Bodman, S. B. Quorum-sensing regulation governs bacterial adhesion, biofilm development, and host colonization in *Pantoea stewartii* subspecies *stewartii*. *Proc. Natl Acad. Sci. USA* **103**, 5983–5988 (2006).
64. Doblas-Ibanez, P. et al. Dominant, heritable resistance to Stewart's wilt in maize is associated with an enhanced vascular defense response to infection with *Pantoea stewartii*. *Mol. Plant Microbe Interact.* **32**, 1581–1597 (2019).
65. Bolger, A. M., Lohse, M. & Usadel, B. Trimmomatic: a flexible trimmer for Illumina sequence data. *Bioinformatics* **30**, 2114–2120 (2014).
66. Kim, D., Landmead, B. & Salzberg, S. L. HISAT: a fast spliced aligner with low memory requirements. *Nat. Methods* **12**, 357–360 (2015).
67. Tarasov, A., Vilella, A. J., Cuppen, E., Nijman, I. J. & Prins, P. Sambamba: fast processing of NGS alignment formats. *Bioinformatics* **31**, 2032–2034 (2015).
68. Liao, Y., Smyth, G. K. & Shi, W. featureCounts: an efficient general purpose program for assigning sequence reads to genomic features. *Bioinformatics* **30**, 923–930 (2014).
69. Anders, S. & Huber, W. Differential expression analysis for sequence count data. *Genome Biol.* **11**, R106 (2010).
70. Kim, D. et al. TopHat2: accurate alignment of transcriptomes in the presence of insertions, deletions and gene fusions. *Genome Biol.* **14**, R36 (2013).
71. Anders, S., Pyl, P. T. & Huber, W. HTSeq—a Python framework to work with high-throughput sequencing data. *Bioinformatics* **31**, 166–169 (2015).
72. Schnable, P. S. et al. The B73 maize genome: complexity, diversity, and dynamics. *Science* **326**, 1112–1115 (2009).
73. Sun, S. et al. Extensive intraspecific gene order and gene structural variations between Mo17 and other maize genomes. *Nat. Genet.* **50**, 1289–1295 (2018).

Acknowledgements

We thank A. Steinbrenner, J. Chan, K. O'Leary, M. Broemmer, H. Riggleman, S. Reyes and S. Delgado for help with planting, treatments and sampling (UCSD); L. Smith (UCSD) for shared UCSD Biology Field Station management; B. Hamberger (Michigan State University) for the *ElHMGR* gene. This work was partially supported by the USDA-ARS National Programs for Food Safety and Plant Genetic Resources, Genomics and Genetic Improvement (to M.M.V., M.G.B. and S.A.C.). Mention of trade names or commercial products in this publication is solely for the purpose of providing specific information and does not imply recommendation or endorsement by the USDA. Research was supported by grants from the National Science Foundation, Division of Integrative Organismal Systems (NSF-IOS) (grant no. 1936492 to B.Y. and grant no. 1546899 to S.P.B.), USDA NIFA AFRI (grant no. 2018-67013-28125 to A.H. and E.S.) for sesquiterpenoids, NSF Plant-Biotic Interactions Program (grant no. 1758976 to E.S. and P.Z.) for diterpenoids, NSF Faculty Early Career Development Program (grant no. 1943591 to A.H.), the DOE Joint Genome Institute Community Science Program (JGI-CSP) (grant nos. CSP 2568 (to P.Z., J.B., E.S. and A.H.) and CSP 503420 (to A.H. and E.S.)) and fellowships provided by the NSF Graduate Research Fellowship Program (to K.M.M.), the U.C. Davis Innovation Institute for Food and Health (IIFH) Fellowship Program (to K.M.M. and P.Z.), the USDA NIFA Predoctoral Fellowship Program (award no. 2019-67011-29544, to K.M.M.) and a Fulbright Research Grant (E0581299, to M.B.).

Author contributions

Y.D., P.R.W., E.P., P.Z., J.S., J.B., K.D., E.A.S. and A.H. designed the experiments and analysed the data. Y.D., E.P., S.A.C., T.G.K., P.Z., K.A.K. and E.S.B. designed, performed and analysed the transcriptome data. Y.D., E.S., A.S.K., K.M.M., P.Z., A.H. and E.A.S. performed MS experiments and MS-related metabolite data analysis. Y.D., E.S., K.M.M., P.Z., E.A.S. and A.H. performed and analysed the enzyme coexpression data. Z.S., A.-D.T. and S.P.B. analysed the combined proteome and transcriptome dataset. T.K. calculated estimates of gene evolution dates. D.R.N. assigned subfamily names for P450 proteins. M.M.V. and M.G.B. generated and analysed the root microbiome data. B.Y., S.N.C. and P.R.W. designed gRNA constructs and generated the *zx1 zx2 zx3* and *zx1 zx2 zx3 zx4* maize mutants. J.S. and M.B. performed metabolite purifications and analysed the NMR data. Y.D. and P.R.W. performed the in vitro and in vivo antibiotic resistance assays. Y.D., P.R.W., E.P., P.Z., E.A.S. and A.H. wrote the manuscript with input from all of the authors.

Competing interests

The authors declare no competing interests.

Additional information

Supplementary information is available for this paper at https://doi.org/10.1038/s41477-020-00787-9.

Correspondence and requests for materials should be addressed to A.H.

Peer review information: *Nature Plants* thanks Peter Balint-Kurti, Hugues Renault and the other, anonymous, reviewer(s) for their contribution to the peer review of this work.

Reprints and permissions information is available at www.nature.com/reprints.

Publisher's note Springer Nature remains neutral with regard to jurisdictional claims in published maps and institutional affiliations.

nature research

Corresponding author(s): Alisa Huffaker

Last updated by author(s): 8/25/2020

Reporting Summary

Nature Research wishes to improve the reproducibility of the work that we publish. This form provides structure for consistency and transparency in reporting. For further information on Nature Research policies, see our Editorial Policies and the Editorial Policy Checklist.

Statistics

For all statistical analyses, confirm that the following items are present in the figure legend, table legend, main text, or Methods section.

n/a	Confirmed	
☐	☒	The exact sample size (*n*) for each experimental group/condition, given as a discrete number and unit of measurement
☐	☒	A statement on whether measurements were taken from distinct samples or whether the same sample was measured repeatedly
☐	☒	The statistical test(s) used AND whether they are one- or two-sided *Only common tests should be described solely by name; describe more complex techniques in the Methods section.*
☒	☐	A description of all covariates tested
☐	☒	A description of any assumptions or corrections, such as tests of normality and adjustment for multiple comparisons
☐	☒	A full description of the statistical parameters including central tendency (e.g. means) or other basic estimates (e.g. regression coefficient) AND variation (e.g. standard deviation) or associated estimates of uncertainty (e.g. confidence intervals)
☐	☒	For null hypothesis testing, the test statistic (e.g. *F*, *t*, *r*) with confidence intervals, effect sizes, degrees of freedom and *P* value noted *Give P values as exact values whenever suitable.*
☒	☐	For Bayesian analysis, information on the choice of priors and Markov chain Monte Carlo settings
☒	☐	For hierarchical and complex designs, identification of the appropriate level for tests and full reporting of outcomes
☐	☒	Estimates of effect sizes (e.g. Cohen's *d*, Pearson's *r*), indicating how they were calculated

Our web collection on statistics for biologists contains articles on many of the points above.

Software and code

Policy information about availability of computer code

Data collection	GC-MS and LC-MS data were collected using Agilent MassHunter Workstation Software vB.08.00. Peptide spectra were acquired using Xcalibur 4.0 (Thermo Scientific) and NMR experiments were conducted on a Bruker Avance III console as well as an Agilent 600-MHz 13C direct detect cryoprobe. qRTPCR data were collected using CFX Manager 3.1 (Bio-Rad) on a Bio-Rad CFX96TM Real-Time PCR Detection System.
Data analysis	Data and statistical analyses were conducted using GraphPad Prism 8.0 (GraphPad Software, Inc.) and JMP Pro 13.0 (SAS Institute Inc). BioEdit v7.0.5 and MEGA7 v7.0.26 were used for phylogenetic analysis. GC-MS and LC-MS data were analyzed using Agilent MassHunter Workstation Software vB.08.00. Peptide data was extracted and analyzed using Spectrum Mill vB.06 (Agilent Technologies). Genome wide association studies were performed initially using the Unified Mixed Linear Model (MLM) in TASSEL 5.0 with final analyses conducted with the R package GAPIT 3.0 using the Compressed MLM. Manhattan plots were constructed in the R package qqman (v0.1.4) (http://cran.r project.org/web/packages/qqman).For comparative gene cluster analyses across inbreds, the genomic sequences of each cluster were extracted and compared using NCBI standalone blastn software, specifically BLAST+ v2.10.1 and further used genoPlotR v0.8.9, MAFFT v7.47 and IQ-TREE v1.6.1216 for final outputs. W22 cDNA concentration was quantified using a fluorometer running Qubit v2.0 firmware to assess and normalize of RNA for RNA-seq analyses. R packages Trimmomatic v0.39, Hisat2 v2.0.0, Sambamba v0.6.8, featureCounts v1.6.4, and DESeq2 were used for 3' RNA-seq data analysis, and R packages, TopHat v2.0.12 and HTSeq v0.6.1, were carried out for the whole transcript RNA-seq data analysis. Weighted Correlation Network Analysis (WGCNA) R package (Version 1.69) was used to cluster genes with similarly expressed proteins and similarly expressed RNA into modules following rank ordering for the W22 time course data. R package topGO (version 2.36.0) was used to find functional enrichment in conjunction with the maize-GAMER data set. R package system PipeR (Version 0.6.1.3) was utilized to predict maize upstream open reading frames. Amplicon sequences from root microbiome profiling were processed with the DADA2 pipeline in R v.3.5. The packages ggplot2 (Version 3.3.2) and pheatmap (Version 1.0.12) were used for root microbiome data analysis. Gene duplication date estimation was carried out using BEAST v2.6.1 and visualized with DensiTree v2.2.7. For the gene duplication date estimation, scripts to perform translation, alignment, and backtranslation as well as data files and BEAST control files have been deposited on GitHub

(https://github.com/TomJKono/Zealexin_Dating).

For manuscripts utilizing custom algorithms or software that are central to the research but not yet described in published literature, software must be made available to editors and reviewers. We strongly encourage code deposition in a community repository (e.g. GitHub). See the Nature Research guidelines for submitting code & software for further information.

Data

Policy information about availability of data

All manuscripts must include a data availability statement. This statement should provide the following information, where applicable:

- Accession codes, unique identifiers, or web links for publicly available datasets
- A list of figures that have associated raw data
- A description of any restrictions on data availability

Publicly available datasets used in the study include the National Center for Biotechnology Information (NCBI) Sequence Read Archive project ID SRP115041 (https://www.ncbi.nlm.nih.gov/sra) and the MaizeGDB BLAST (https://maizegdb.org/popcorn/main/index.php) database. Raw read sequences have been deposited in the NCBI Gene Expression Omnibus (http://www.ncbi.nlm.nih.gov/geo/) under the accession numbers GSE138961 and GSE138962. Raw sequence data from the root microbiome are available at NCBI BioProject (https://www.ncbi.nlm.nih.gov/bioproject/) accession number PRJNA580260. Raw proteomic mass spectra have been deposited at the Mass Spectrometry Interactive Virtual Environment repository (ftp://massive.ucsd.edu/MSV000084285). Maize related germplasm used in this research have been previously described (1-7) and can be obtained from United State Department of Agriculture Germplasm Resources Information Network (https://www.ars-grin.gov) and the Maize Genetics Cooperation Stock Center (http://maizecoop.cropsci.uiuc.edu). Where possible, gene identifiers used throughout the manuscript were in reference to B73 RefGen_v4 (https://www.maizegdb.org/genome/assembly/Zm-B73-REFERENCE-GRAMENE-4.0) which served as a foundation of the study. All figures have associated raw data available upon request.

References to detailed description of germplasm used:

1 Lee, M. et al. Expanding the genetic map of maize with the intermated B73 x Mo17 (IBM) population. Plant Mol. Biol. 48, 453-461 (2002).
2 Flint-Garcia, S. A. et al. Maize association population: a high-resolution platform for quantitative trait locus dissection. Plant J. 44, 1054-1064 (2005).
3 McMullen, M. D. et al. Genetic Properties of the Maize Nested Association Mapping Population. Science 325, 737-740 (2009).
4 Schnable, P. S. et al. The B73 maize genome: complexity, diversity, and dynamics. Science 326, 1112-1115 (2009).
5 Eichten, S. R. et al. B73-Mo17 Near-Isogenic Lines Demonstrate Dispersed Structural Variation in Maize. Plant Physiol. 156, 1679-1690 (2011).
6 Springer, N. M. et al. The maize W22 genome provides a foundation for functional genomics and transposon biology. Nat. Genet. 50, 1282-1288 (2018).
7 Sun, S. et al. Extensive intraspecific gene order and gene structural variations between Mo17 and other maize genomes. Nat. Genet. 50, 1289-1295 (2018).

Field-specific reporting

Please select the one below that is the best fit for your research. If you are not sure, read the appropriate sections before making your selection.

☒ Life sciences ☐ Behavioural & social sciences ☐ Ecological, evolutionary & environmental sciences

For a reference copy of the document with all sections, see nature.com/documents/nr-reporting-summary-flat.pdf

Life sciences study design

All studies must disclose on these points even when the disclosure is negative.

Sample size	No specific statistical methods were used to determine sample size for the experiments reported in this manuscript. Instead, sample sizes were chosen based on our previous experience in with maize and tobacco, variability encountered, availability of plants and space considerations. Unstressed maize plants produce exceedingly low levels of zealexins and fungal elicitation elicits highly consistent qualitative and quantitative differences in production. With a broad dynamic range in zealexin accumulation following elicitation, a modest number of biological replicates are sufficient to detect differences. In every case, a sample size of at least 3 independent biological replicates was selected for purposes of statistical comparisons. These sample sizes proved to be sufficient to detect significant differences between treatments / genotypes and to obtain reproducible results in independent runs of the same experiment.
Data exclusions	No data were excluded from analysis in this study.
Replication	When technical problems were eliminated and methods described were followed all experiments could be reliably reproduced. All experiments were conducted at least two times. The independent experimental replications gave similar results.
Randomization	In this study, maize and tobacco plants were used as the dominant model organisms. Plants were grown in the field, greenhouse and growth chambers and randomly used for experiments.
Blinding	Initial RNA-seq data analyses were done blind. Also blinding was performed for the forward genetic studies and all biochemical analyses. In these cases, plants and plant analytical samples were assigned a simple numerical series for each experiment and the identities of the samples/results were not revealed until final analyses of processed data. Regarding Nicotiana benthamiana plants used for the Agrobacterium mediated heterologous expression of enzymes, blinding was not attempted due to the large number of chemicals, solutions, and vectors that had to be prepared and precisely combined for the plant treatments. While blinding was not practical during treatments, subsequent downstream steps were performed blinded with samples reduced to a simple numerical series and processed by different team members.

Reporting for specific materials, systems and methods

We require information from authors about some types of materials, experimental systems and methods used in many studies. Here, indicate whether each material, system or method listed is relevant to your study. If you are not sure if a list item applies to your research, read the appropriate section before selecting a response.

Materials & experimental systems

n/a	Involved in the study
☒	☐ Antibodies
☒	☐ Eukaryotic cell lines
☒	☐ Palaeontology and archaeology
☒	☐ Animals and other organisms
☒	☐ Human research participants
☒	☐ Clinical data
☒	☐ Dual use research of concern

Methods

n/a	Involved in the study
☒	☐ ChIP-seq
☒	☐ Flow cytometry
☒	☐ MRI-based neuroimaging